The Astrophysical Journal Letters, 971:L51 (27pp), 2024 August 20 https://doi.org/10.3847/2041-8213/ad64d1

Host Galaxies for Four Nearby CHIME/FRB Sources and the Local Universe FRB Host Galaxy Population

Mohit Bhardwaj[1,2,3], Daniele Michilli[4,5], Aida Yu. Kirichenko[6], Obinna Modilim[5], Kaitlyn Shin[4,5], Victoria M. Kaspi[2,3], Bridget C. Andersen[2,3], Tomas Cassanelli[7], Charanjot Brar[2,3], Shami Chatterjee[8], Amanda M. Cook[9,10], Fengqiu Adam Dong[11], Emmanuel Fonseca[12,13], B. M. Gaensler[9,10,25], Adaeze L. Ibik[9,10], J. F. Kaczmarek[14], Adam E. Lanman[4,5], Calvin Leung[15,16], K. W. Masui[4,5], Ayush Pandhi[9,10], Aaron B. Pearlman[2,3,17,18,19], Emily Petroff[20], Ziggy Pleunis[9], J. Xavier Prochaska[21,22,23], Masoud Rafiei-Ravandi[2,3], Ketan R. Sand[2,3], Paul Scholz[9,24], and Kendrick M. Smith[20]

[1] McWilliams Center for Cosmology and Astrophysics, Department of Physics, Carnegie Mellon University, Pittsburgh, PA 15213, USA; mohitb@andrew.cmu.edu
[2] Trottier Space Institute, McGill University, 3550 rue University, Montréal, QC H3A 2A7, Canada
[3] Department of Physics, McGill University, 3600 rue University, Montréal, QC H3A 2T8, Canada
[4] MIT Kavli Institute for Astrophysics and Space Research, Massachusetts Institute of Technology, 77 Massachusetts Ave., Cambridge, MA 02139, USA
[5] Department of Physics, Massachusetts Institute of Technology, 77 Massachusetts Ave., Cambridge, MA 02139, USA
[6] Instituto de Astronomía, Universidad Nacional Autónoma de México, Apdo. Postal 877, Ensenada, Baja California 22800, México
[7] Department of Electrical Engineering, Universidad de Chile, Av. Tupper 2007, Santiago 8370451, Chile
[8] Cornell Center for Astrophysics and Planetary Science, Cornell University, Ithaca, NY 14853, USA
[9] Dunlap Institute for Astronomy & Astrophysics, University of Toronto, 50 St. George Street, Toronto, ON M5S 3H4, Canada
[10] David A. Dunlap Department of Astronomy & Astrophysics, University of Toronto, 50 St. George Street, Toronto, ON M5S 3H4, Canada
[11] Dept. of Physics and Astronomy, 6224 Agricultural Road, Vancouver, BC V6T 1Z1, Canada
[12] Center for Gravitational Waves and Cosmology, West Virginia University, Chestnut Ridge Research Building, Morgantown, WV 26505, USA
[13] Department of Physics and Astronomy, West Virginia University, P.O. Box 6315, Morgantown, WV 26506, USA
[14] CSIRO Space & Astronomy, Parkes Observatory, P.O. Box 276, Parkes NSW 2870, Australia
[15] Department of Astronomy, University of California Berkeley, Berkeley, CA 94720, USA
[16] NASA Hubble Fellowship Program (NHFP) Einstein Fellow
[17] Banting Fellow
[18] McGill Space Institute Fellow
[19] Fonds de Recherche du Quebec—Nature et Technologies (FRQNT) Postdoctoral Fellow
[20] Perimeter Institute for Theoretical Physics, 31 Caroline Street N, Waterloo, ON N2L 2Y5, Canada
[21] Department of Astronomy and Astrophysics, University of California, Santa Cruz, Santa Cruz, CA 95064, USA
[22] Kavli Institute for the Physics and Mathematics of the Universe (Kavli IPMU), 5-1-5 Kashiwanoha, Kashiwa, 277-8583, Japan
[23] Division of Science, National Astronomical Observatory of Japan, 2-21-1 Osawa, Mitaka, Tokyo 181-8588, Japan
[24] Department of Physics and Astronomy, York University, 4700 Keele Street, Toronto, ON MJ3 1P3, Canada
Received 2023 October 15; revised 2024 July 15; accepted 2024 July 16; published 2024 August 20

Abstract

We present the host galaxies of four apparently nonrepeating fast radio bursts (FRBs), FRB 20181223C, FRB 20190418A, FRB 20191220A, and FRB 20190425A, reported in the first Canadian Hydrogen Intensity Mapping Experiment (CHIME/FRB) catalog. Our selection of these FRBs is based on a planned hypothesis testing framework where we search all CHIME/FRB Catalog-1 events that have low extragalactic dispersion measure ($<100\,\mathrm{pc\,cm^{-3}}$), with high Galactic latitude ($|b|>10^{\circ}$) and saved baseband data. We associate the selected FRBs with galaxies with moderate to high star formation rates located at redshifts between 0.027 and 0.071. We also search for possible multimessenger counterparts, including persistent compact radio and gravitational-wave sources, and find none. Utilizing the four FRB hosts from this study, along with the hosts of 14 published local Universe FRBs ($z<0.1$) with robust host association, we conduct an FRB host demographics analysis. We find all 18 local Universe FRB hosts in our sample to be spirals (or late-type galaxies), including the host of FRB 20220509G, which was previously reported to be elliptical. Using this observation, we scrutinize proposed FRB source formation channels and argue that core-collapse supernovae are likely the dominant channel to form FRB sources. Moreover, we infer no significant difference in the host properties of repeating and apparently nonrepeating FRBs in our local Universe FRB host sample. Finally, we find the burst rates of these four apparently nonrepeating FRBs to be consistent with those of the sample of localized repeating FRBs observed by CHIME/FRB. Therefore, we encourage further monitoring of these FRBs with more sensitive radio telescopes.

Unified Astronomy Thesaurus concepts: Radio transient sources (2008); Supernovae (1668); Spiral galaxies (1560); Neutron stars (1108); Pulsars (1306); Radio bursts (1339); Transient sources (1851)

1. Introduction

Fast radio bursts (FRBs) are energetic transients of coherent radio emission that last for ∼few milliseconds (Lorimer et al. 2007; Thornton et al. 2013) and are observed out to cosmological distances (for more details, see Petroff et al. 2022). Since the discovery of the first FRB in 2007,

[25] Present address: Division of Physical and Biological Sciences, University of California Santa Cruz, Santa Cruz, CA 95064, USA.

~1000 FRBs have been reported to date.[26] However, their origin continues to be a subject of intense debate. So far, extragalactic FRBs have exclusively manifested as radio phenomena. Consequently, given the lack of prompt or afterglow counterparts at other wavelengths, it becomes imperative to investigate their host galaxies and local surroundings to unravel their sources (Heintz et al. 2020; Bhandari et al. 2022; Gordon et al. 2023). For example, analyzing the local environment of FRBs can help in understanding the necessary conditions for the formation of their sources (Bassa et al. 2017; Marcote et al. 2020; Mannings et al. 2021; Tendulkar et al. 2021).

Numerous models have been proposed to explain the origins of FRBs, encompassing both cataclysmic and noncataclysmic formation channels (for a review of FRB models, see Platts et al. 2019). However, because of the high volumetric rate of FRBs (Luo et al. 2020; Hashimoto et al. 2022; Shin et al. 2023), it is likely that most FRBs are repeating sources (Ravi 2019; Bhardwaj et al. 2021b; James 2023). Moreover, the majority of proposed source models invoke young, highly magnetized neutron stars as FRB sources (Zhang 2023). The neutron star origin hypothesis gained strong support after the discovery of radio bursts from the Galactic magnetar SGR 1935+2154 (Bochenek et al. 2020; CHIME/FRB Collaboration et al. 2020), which is reminiscent of FRBs. It is interesting to note that SGR 1935+2154 is likely formed via core-collapse supernovae (CCSNe; Kothes et al. 2018), one of the prompt formation channels proposed for FRB sources (Zhang 2023). Moreover, several other Galactic magnetars are found in SN remnants, e.g., 1E 2259+586 or 1E 1841−045, which supports this argument.[27]

However, the recent discovery of a repeating FRB, FRB 20200120E (Bhardwaj et al. 2021a), in an old globular cluster (GC) of the galaxy M81 challenges this hypothesis and suggests the possibility of dynamically forming FRB sources in dense cluster cores through delayed formation channels (Kirsten et al. 2022), such as accretion-induced collapse of white dwarfs and binary white dwarf mergers (Kremer et al. 2021a).

It is also conceivable that both delayed and prompt formation channels contribute to the population of FRB sources. This notion finds support in the observation that FRBs have been identified across a wide range of galactic environments, encompassing both actively star-forming galaxies and quiescent ones. The diversity within these host environments implies a broad range of potential formation timescales for the FRB sources (Gordon et al. 2023; Law et al. 2024). However, it is important to note that existing FRB host demographic studies have not yet taken into consideration potential biases arising from radio and optical selection effects. These biases could potentially influence the core conclusions drawn from such studies (Seebeck et al. 2021; Jahns-Schindler et al. 2023). Nevertheless, a statistically significant sample of localized FRBs, especially those located in the local Universe ($z \lesssim 0.1$), will be important for testing various proposed FRB formation channels, where the effects of biases either are relatively smaller than for those at larger redshifts (Ocker et al. 2022) or can be studied more robustly. Due to the limited sensitivity of current telescopes, in-depth study of FRB local environments is mainly possible for nearby sources. Consequently, realizing the complete potential of multiwavelength and multimessenger follow-ups depends on the proximity of FRBs. This facilitates endeavors such as detecting prompt X-ray emission from FRB sources, a prediction of almost all magnetar-based models (Scholz et al. 2020; Pearlman et al. 2023). Therefore, local Universe FRBs are inarguably the best sources to uncover the origins of FRBs.

The Canadian Hydrogen Intensity Mapping Experiment Fast Radio Burst (CHIME/FRB) Project (CHIME/FRB Collaboration et al. 2018) published its first catalog (hereafter denoted as Catalog-1) of 536 FRBs detected between 400 and 800 MHz from 2018 July 25 to 2019 July 1, including 62 bursts from 18 previously reported repeating sources (CHIME/FRB Collaboration et al. 2021). The detected FRBs show dispersion measures (DMs) ranging between 102 and 3037 pc cm^{-3}. However, most of the Catalog-1 FRBs are not localized to their hosts because the CHIME/FRB real-time pipeline processes can localize FRBs to a sky region of around a few tens of arcminutes, which is not sufficient to robustly identify FRB host galaxies (Eftekhari & Berger 2017). Moreover, only three Catalog-1 FRBs, all of which are repeating sources in the local Universe with low extragalactic DM, namely, FRB 20181030A, FRB 20180814A, and FRB 20190303A (CHIME/FRB Collaboration et al. 2019; Fonseca et al. 2020), have been localized to their host galaxies (Marcote et al. 2020; Bhardwaj et al. 2021b; Michilli et al. 2023) using the CHIME/FRB baseband localization pipeline (Michilli et al. 2021).

In this study, we present a systematic search for the host galaxies of FRBs reported in CHIME/FRB Catalog-1. Our methodology for selecting Catalog-1 FRBs, as detailed in Section 2.1, identifies FRBs characterized primarily by their low DM excess and saved baseband data. Following this methodology, we identify four apparently nonrepeating FRBs and find only one plausible host galaxy candidate within each of their respective baseband localization regions as described in Section 2.2. Furthermore, the chance association probability of the identified plausible host galaxies, as explained in Section 2.3, remains below 10%, even after accounting for the look-elsewhere effect. After identifying likely hosts of the four Catalog-1 FRBs, we detail our search for multimessenger and multiwavelength counterparts, including compact persistent radio sources, in Section 2.5. In Section 3.1, we discuss the implication of the localized nearby FRB host sample ($z < 0.1$), which includes the four hosts presented in this study, and determine the dominant formation channel of FRB sources. Additionally, we report on a burst rate analysis for the four FRBs in Section 3.2. Finally, we summarize and conclude in Section 4.

We adopt the Planck Collaboration et al. (2020) cosmology with $H_0 = 67.7\,\mathrm{km\,s^{-1}\,Mpc^{-1}}$.

2. Observations and Results

2.1. CHIME/FRB Sample Selection

In this section, we describe the formalism adopted for selecting Catalog-1 FRBs for our host association study. It is worth noting that not all baseband-localized FRBs can be associated robustly with a galaxy (see, e.g., Michilli et al. 2021; Ibik et al. 2024). Therefore, looking for hosts of every Catalog-

[26] For a complete list of known FRBs, see https://www.herta-experiment.org/frbstats/ (Spanakis-Misirlis 2021) or the TNS: https://www.wis-tns.org/ (Yaron et al. 2020).

[27] See https://www.physics.mcgill.ca/~pulsar/magnetar/main.html or Olausen & Kaspi (2014).

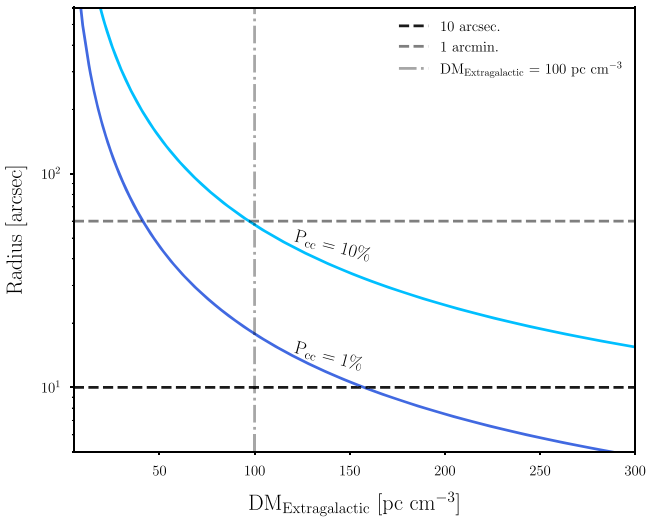

Figure 1. Probability curves for $P_{cc} = 0.01$ and 0.1 as a function of extragalactic DM (or excess DM) and localization radius for the faintest FRB host discovered to date ($M_r = -17$ AB mag). Note that an FRB with an extragalactic DM ≈ 100 pc cm^{-3} can be associated with a dwarf, star-forming galaxy, like the FRB 20121102A host, with P_{cc} of 0.01 and 0.1 using a localization precision of $\approx 10''$ and $1'$, respectively. The plot is produced using the formalism discussed in Section 2.1.

1 FRB that has a baseband localization is not an optimal strategy. Moreover, this would further result in decreasing the statistical power of finding promising FRB hosts when we correct for the look-elsewhere effect in order to avoid false positives. Therefore, we have opted for a planned hypothesis testing framework wherein we select Catalog-1 FRBs based on predefined criteria. These criteria are as follows:

1. Existence of baseband localization with 1σ precision $\lesssim 1'$.
2. The DM excess of the FRB should be $\leqslant 100$ pc cm^{-3}, i.e., DM $-$ max(DM(MW; NE2001, YMW16) $\leqslant 100$ pc cm^{-3}, where NE2001 (Cordes & Lazio 2002) and YMW16 (Yao et al. 2017) are two widely used Galactic disk electron density distribution models.
3. The FRB should not be behind the Galactic plane (Galactic latitude $|b| > 10°$).

The rationale for criteria 1 and 2 is as follows: As the maximum distance to the FRB hosts can be reasonably estimated from their DM excesses, FRBs with low DM excess are expected to be nearby sources. For instance, using the average macquart relation (Macquart et al. 2020), an FRB with a DM excess of 100 pc cm^{-3} would have a maximum redshift of 0.1. If this low DM excess FRB is localized using the CHIME/FRB baseband pipeline (Michilli et al. 2021) to a localization region of radius $\sim 1'$, the number density of galaxies as faint as the faintest FRB host discovered to date (FRB 20121102A with absolute r-band magnitude $M_r = -17$ AB mag; Tendulkar et al. 2017) is expected to be small (Eftekhari & Berger 2017), hence making any plausible association with such a host a rare coincidence ($P_{cc} \leqslant 10\%$; the generally accepted threshold in the FRB community; see Heintz et al. 2020; Bhandari et al. 2022). This is shown in Figure 1. Therefore, CHIME/FRB baseband localizations are most promising to identify the host galaxies of low-DM FRB events (DM excess $\leqslant 100$ pc cm^{-3}). Moreover, this low DM excess cutoff has an additional advantage. At $z = 0.1$, the faintest FRB host discovered to date, FRB 20121102A, would have an apparent r-band magnitude of $\lesssim 21$ AB mag. There are several archival wide-sky optical surveys, such as the Sloan Digital Sky Survey (SDSS; Abdurro'uf et al. 2022), the Panoramic Survey Telescope and Rapid Response System (Pan-STARRS) survey (Chambers et al. 2016), and the Dark Energy Spectroscopic Instrument (DESI) survey (DESI Collaboration et al. 2016), which are sufficiently deep to detect galaxies of r-band magnitude $\leqslant 21$ AB mag. Therefore, the hosts of nearby FRBs can be identified in the aforementioned archival optical survey data. We note that the choice of 100 pc cm^{-3} is rather conservative, as this excess includes the contributions from the FRB host and Milky Way circumgalactic medium (CGM). Assuming the FRB 20200120E DM excess of approximately 40 pc cm^{-3} from Bhardwaj et al. (2021a) as a conservative estimate of the FRB host and Milky Way CGM contribution (since the FRB is localized to a GC at a large offset (20 kpc) from the M81 galaxy center), the resulting contribution from the intergalactic medium would be 60 pc cm^{-3} according to our cutoff. This leads to a 90% confidence upper bound on the maximum redshift, which is <0.1, based on the study by James et al. (2022) that attempts to quantify potential scatter in the Mcquart relation. Finally, from Figure 1, we note that it is possible to identify host galaxies with DM excess $\lesssim 300$ pc cm^{-3} with the baseband localization precision of $\lesssim 20''$. This will be explored in our future low-DM FRB localization papers.

Lastly, the inclusion of the final criterion, i.e., $|b| > 10°$, is justified by the significant uncertainty in Milky Way DM models along Galactic plane sight lines (Price et al. 2021; Ravi et al. 2023b).

Using these preplanned criteria, we can evade the effect of the multiple testing problem or p-value hacking (Vidgen & Yasseri 2016), which makes our host associations more robust.

Based on these criteria, we identify four Catalog-1 CHIME FRBs: FRB 20181223C, FRB 20190418A, FRB 20191220A, and FRB 20190425A. We then run the CHIME/FRB baseband pipeline on the saved baseband data of these FRBs and estimate their baseband localization regions. The procedure used to estimate the baseband localizations is detailed by Michilli et al. (2021, 2023). The dedispersed baseband data waterfall plots and major characteristics of the four FRBs are shown in Figure 2 and Table 1, respectively. Other burst properties, such as fluence and flux density, along with a detailed description of the baseband data analysis of these FRBs, will be presented elsewhere. Next, we describe the host identification procedure used in this work.

2.2. Host Galaxy Search

First, we argue below that all four FRBs are unlikely to be Galactic in origin. As shown in Table 1, the DM excess along respective FRB sight lines is >50 pc cm^{-3}. This remains true even after accounting for the fiducial MW halo DM contribution of 30 pc cm^{-3} using the MW halo DM model proposed by Yamasaki & Totani (2020); for more discussion on this, see Cook et al. (2023). Moreover, there is no cataloged Galactic ionized region (Anderson et al. 2014), molecular complex (Dame et al. 2001), satellite galaxy (Kaisina et al. 2019; Karachentsev & Kaisina 2019), or Galactic GC (Harris 2010; Gaia Collaboration et al. 2018; Vasiliev 2019) in the direction of the FRBs that can account for their observed FRB DM excess. Therefore, we argue for the extragalactic association of all four FRBs. Next, for the purpose of finding

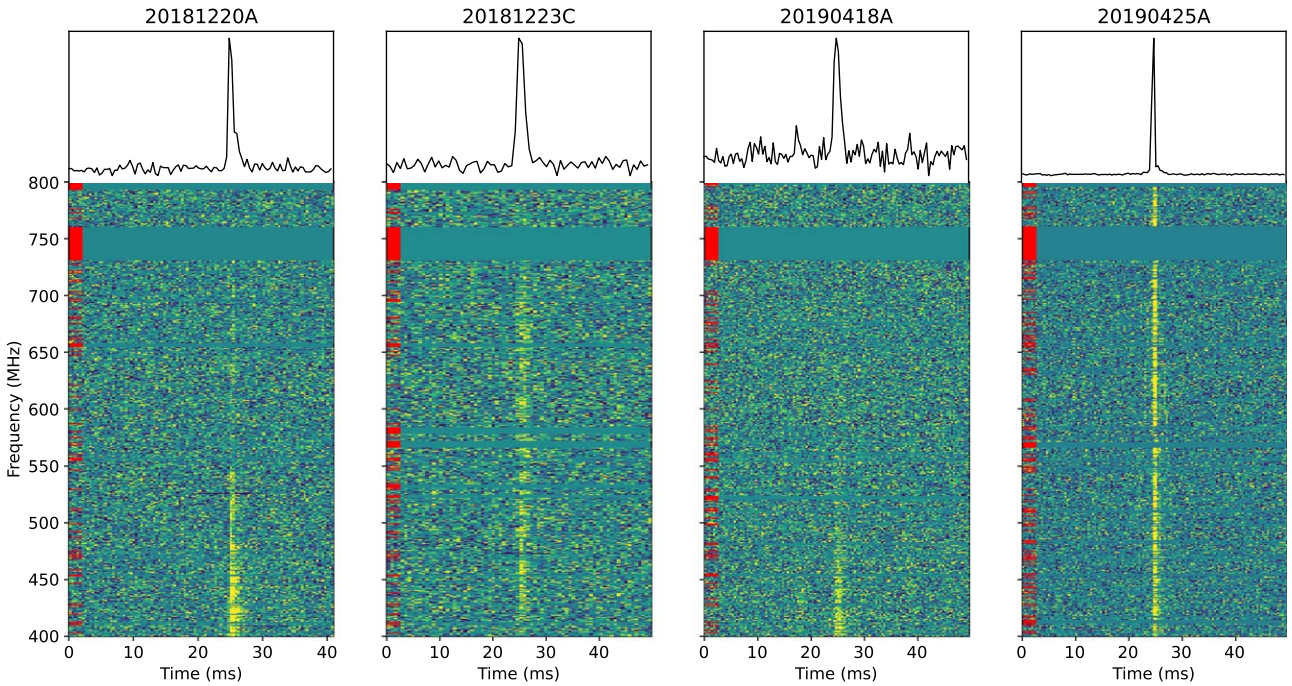

Figure 2. Frequency vs. time ("waterfall") plots of the dedispersed bursts detected from FRB 20181220A, FRB 20181223C, FRB 20190418A, and FRB 20190425A with saved baseband data. See Table 1 for their major burst properties. The waterfall plots are binned to have a temporal resolution of 0.39 ms and a spectral resolution of 0.391 MHz. Red lines represent bad frequency channels that were flagged in this analysis.

all promising FRB host galaxies, we estimate the 90% credible upper limit on the maximum redshift of the four FRBs using the formalism discussed by Bhardwaj et al. (2021b). Those values are reported in Table 1.

We now report on our search for the host galaxies of four selected FRBs using archival data from Pan-STARRS. We employ the Pan-STARRS1 Source Types and Redshifts with Machine Learning (PS1−STRM) catalog (Beck et al. 2021) to identify plausible host galaxy candidates. The Pan-STARRS data set is chosen because it covers the field of view (FOV) of all four FRBs, ensuring uniformity, and is complete to detect the faintest known FRB host at the maximum redshift of these FRBs, as discussed in Section 2.1.

2.2.1. FRB 20181220A

The Pan-STARRS r-image of the FRB 2σ localization region is shown in Figure 3. Using the PS1−STRM catalog, we found only one galaxy, PSO J231447.57+482031.6, within the 2σ baseband localization region of the FRB that satisfies our r-band constraint ($\leqslant$21 AB mag). The galaxy was first reported in the Two Micron All Sky Survey (2MASS) selected flat galaxy catalog as 2MFGC 17440 (Mitronova et al. 2004) and classified as an Scd-type spiral using the observed morphology of the galaxy in 2MASS data (Mitronova & Korotkova 2015).

The spectroscopic redshift of 2MFGC 17440 is unavailable in any of the following major public astronomy databases: NASA/IPAC Extragalactic Database (NED; Mazzarella & NED Team 2017), Set of Identifications, Measurements, and Bibliography for Astronomical Data (SIMBAD; Wenger et al. 2000), and VizieR.[28] Therefore, we conducted spectroscopic observations on 2020 August 11 (Program ID: GN-2020B-FT-201) using the Gemini Multi-Object Spectrograph (GMOS) on the Gemini North telescope. Spectroscopy of the galaxy was reduced using the `PypeIt` reduction package (Prochaska et al. 2020). This package employs optimal extraction techniques to generate a 1D spectrum from the flat-fielded and sky-subtracted 2D spectral images of the field. For flux calibration using `PypeIt`, we used the spectrophotometric standard star G191-B2B (Massey et al. 1995) from the compilation of associated calibration observations accessible through the Gemini Observatory Archive Portal.[29] We then fitted the calibrated 1D spectrum using the `Specutils` package (Earl et al. 2023) and estimated the galaxy's spectroscopic redshift $z_{\rm spec} = 0.02746(3)$ based on the Hα, [N II], and [S II] line features. The fitted 1D spectra with a subset of these lines are shown in Figure 4. From the fitted spectrum, we estimate an Hα flux density $= (2.16 \pm 0.18) \times 10^{-13}$ erg s^{-1}, which we use to estimate the star formation rate (SFR) of the galaxy as noted in Table 2.

2.2.2. FRB 20181223C

The Pan-STARRS r-band image of the FRB 2σ localization region is shown in Figure 3. From the PS1−STRM catalog, we identified four host galaxy candidates (Sources 1, 2, 3, and 4 in Figure 3) within the FRB's 2σ baseband localization region, all meeting our r-band constraint. Among these candidates, only PSO J120340.98+273251.4 satisfies the maximum redshift criterion ($z < z_{\rm max}$; see Table 1) based on its photometric redshift. To confirm this, we obtained spectroscopic redshifts for the four galaxies using multiobject spectroscopic observations conducted with the 10.4 m Gran Telescopio Canarias (GTC), as detailed in Appendix B. Our GTC observations confirm PSO J120340.98+273251.4 at $z_{\rm spec} = 0.03024 \pm 0.00001$ as the only galaxy within the field that satisfies the maximum redshift constraint, suggesting that it is the likely host of the FRB.

[28] https://vizier.cds.unistra.fr/viz-bin/VizieR

[29] https://archive.gemini.edu/

Table 1
Major Observables of the Selected CHIME FRBs

Parameter	FRB 20181220A	FRB 20181223C	FRB 20190418A	FRB 20190425A
R.A. (J2000)[a]	$23^h14^m52^s$	$12^h03^m43^s$	$04^h23^m16^s$	$17^h02^m42^s$
σ(R.A.) (arcsec)[a]	28	23	27	11
Decl. (J2000)[a]	48°20′25″	27°33′09″	16°04′02″	21°34′35″
σ(decl.) (arcsec)[a]	20	26	34	12
l, b (deg, deg)	106.82, −11.49	207.90, +79.40	179.30, −22.89	42.10, +33.08
DM[b] (pc cm^{-3})	209.4	112.5	184.5	128.2
$DM_{MW,NE2001}$[c] (pc cm^{-3})	126	20	71	49
$DM_{MW,YMW16}$[c] (pc cm^{-3})	123	20	86	39
Max. redshift (z_{max})[d]	0.096	0.085	0.12	0.081
Exposure[e] (hr)	71 ± 2	64 ± 3	68 ± 1	67 ± 2

Notes.
[a] Baseband localization region of the FRB along with 1σ uncertainty.
[b] From CHIME/FRB Collaboration et al. (2019).
[c] Maximum DM model prediction along this line of sight for the NE2001 (Cordes & Lazio 2002) and YMW16 (Yao et al. 2017) Galactic disk electron density distribution models.
[d] Estimated 90% credible region upper limit estimated using the formalism discussed by Bhardwaj et al. (2021b).
[e] Total exposure for the upper transit of each source. The uncertainty in the exposure values is dominated by the corresponding source decl. uncertainties since the widths of the synthesized beams vary significantly with decl.

We find the optical spectrum of the galaxy in the SDSS DR17 database (Abdurro'uf et al. 2022).[30] The galaxy is classified as a star-forming spiral (Simard et al. 2011; Domínguez Sánchez et al. 2018). The notable physical properties of the galaxy from the SDSS database are presented in Table 2.

2.2.3. FRB 20190418A

We searched the PS1−STRM catalog for potential host candidates that meet our r-band constraint and found only one galaxy within the 2σ localization region of the FRB: PSO J042314.96+160425.6. The Pan-STARRS r-image of the FRB 2σ localization region is shown in Figure 3. Moreover, while searching for deeper images, we found that the galaxy is also cataloged in the UKIDSS-DR9 GCS survey data release (Lawrence et al. 2007) and has Petrosian K-band magnitude 14.42 ± 0.04 mag (this is used in our `Prospector` analysis; see Appendix A). In the UKIDSS-DR9 GCS K-band data, the galaxy shows spiral-arm-like features, making it likely a spiral galaxy.

As the spectroscopic redshift of the galaxy is not available in the public databases stated above, we conducted spectroscopic observations of PSO J042314.96+160425.6 with the MOS instrument on the Gemini North telescope on 2021 December 10 (Program ID = GN-2021B-Q-115). Spectroscopy was then reduced using the `PypeIt` reduction package (Prochaska et al. 2020), which optimally extracts a 1D spectrum from the flat-fielded and sky-subtracted 2D spectral image. For flux calibration within the framework of `PypeIt`, we used the spectrophotometric standard Feige 34 (Oke 1990), which was observed 3 days after the target. The calibrated 1D spectrum was then fitted using the `Specutils` package as shown in Figure 4, which yields a spectroscopic redshift of $z_{spec} = 0.07132(1)$ based on the Hα, [N II], and [S II] line features. We also estimate an Hα flux density = $(2.3 \pm 0.3) \times 10^{-15}$ erg s^{-1}, which we use to estimate the SFR of the galaxy as noted in Table 2.

[30] https://dr12.sdss.org/spectrumDetail?plateid=2226&mjd=53819&fiber=0509

2.2.4. FRB 20190425A

We searched for potential host candidates in the PS1−STRM catalog within the 2σ localization region of the FRB shown in Figure 3 and find only one galaxy, UGC 10667. UGC 10667 is a star-forming Sbc-type spiral galaxy (Hernández-Toledo et al. 2010) located at $z_{spec} = 0.03122 \pm 0.00001$ (Abdurro'uf et al. 2022) estimated in the SDSS DR17 catalog. The notable physical properties of the galaxy from the SDSS database are presented in Table 2. We note that Panther et al. (2023) found this galaxy to be the most probable host of FRB 20190425A using the CHIME/FRB header localization region (precision ∼10′; CHIME/FRB Collaboration et al. 2021) and Probabilistic Association of Transients to Hosts (PATH) package (Aggarwal et al. 2021; $P(O|x) = 0.79$).

Although we have identified only one potential host galaxy candidate within the 2σ localization region of each of the four FRBs, claiming them as host galaxies requires validating that their presence is not a mere fortuitous alignment. To address this, we next estimate the probability of chance association for the identified host galaxy candidates.

2.3. Chance Association Probability

In accordance with established practices for estimating chance association probabilities (P_{cc}) for various astrophysical transients (e.g., Bloom et al. 2002; Bell et al. 2015; Blanchard et al. 2016), we calculate P_{cc} based on the angular separation between the FRB position and the center of a potential host galaxy, considering the uncertainty of the FRB's baseband localization region and the apparent magnitude of the galaxy. For a more comprehensive discussion, refer to Eftekhari & Berger (2017). In essence, the derivation of P_{cc} relies on galaxy counts brighter than a certain magnitude threshold, accounting for the prevalence of faint galaxies on the sky. We adopt a Poisson distribution of galaxies across the sky and compute the likelihood of encountering one or more galaxies with apparent r-band magnitude (m_r) equal to or less than that of the host galaxy by chance, within the 2σ baseband localization region of the FRB. Using the areal number density of FRB host galaxies based on the formalism discussed by Driver et al.

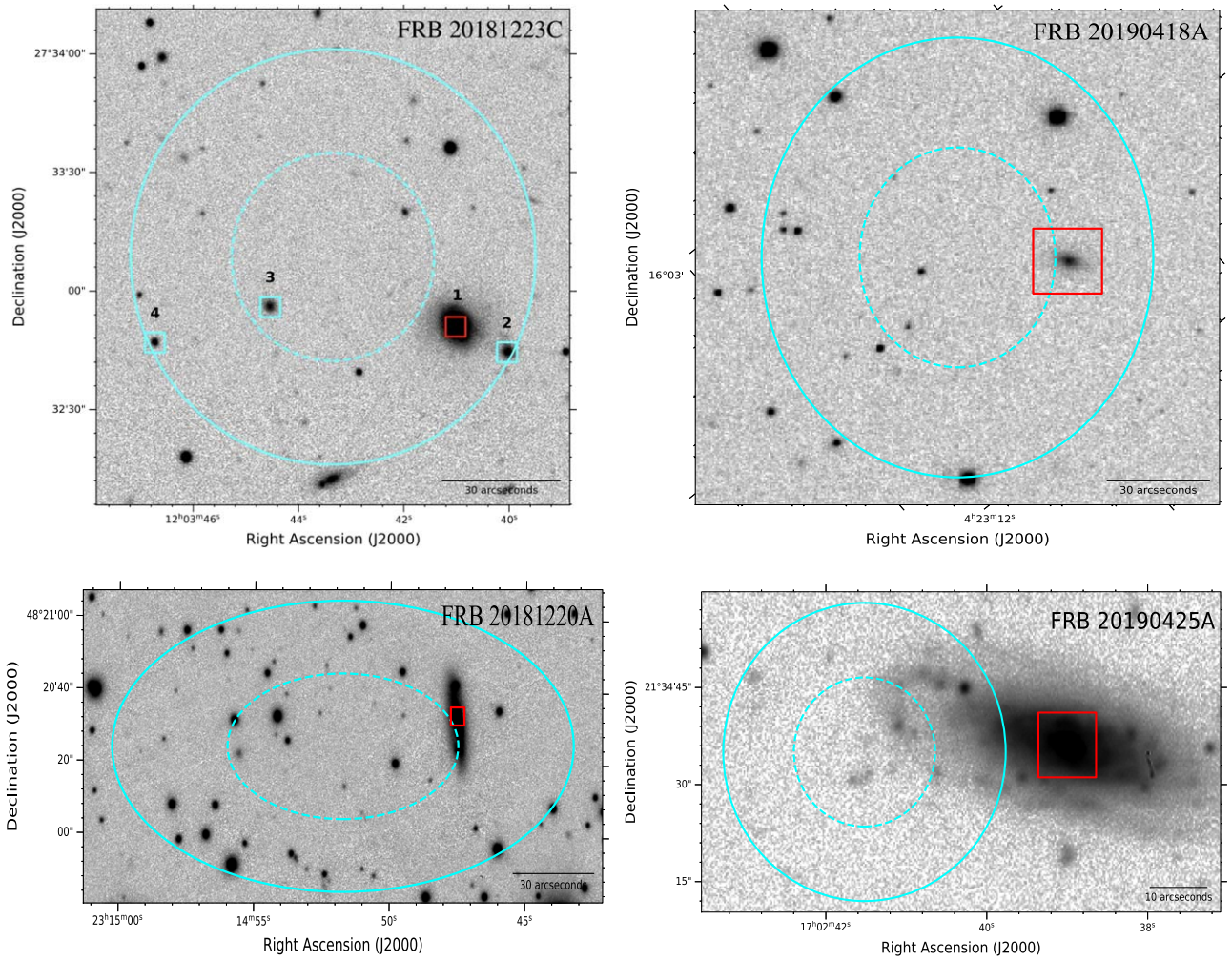

Figure 3. Pan-STARRS r-band images of the baseband localization regions for FRB 20181223C (top left), FRB 20190418A (top right), FRB 20181220A (bottom left), and FRB 20190425A (bottom right). The 1σ and 2σ baseband localization regions are represented by dotted and solid cyan ellipses, respectively. While only one plausible host galaxy candidate is identified for FRB 20181220A, FRB 20190418A, and FRB 20190425A, we identify four potential host galaxy candidates within the localization area of FRB 20181223C. However, following our multiobject spectroscopic analysis discussed in Appendix B, only one galaxy satisfies the estimated maximum redshift limit for FRB 20181223C. Note that the bright disk galaxy (bottom middle) just outside the 2σ region is a spiral galaxy at $z_{\rm spec} = 0.347$, well above the maximum redshift estimated for FRB 20181223C, i.e., $z_{\rm max} = 0.085$ (see Table 1). Finally, the most probable host galaxies for the four FRBs are delineated by red boxes.

(2016), we estimate $P_{\rm cc}$ using Equation (2) from Eftekhari & Berger (2017). The estimated $P_{\rm cc}$ value for the proposed host galaxies of the four FRBs are presented in Table 2. Next, we apply a correction to the estimated $P_{\rm cc}$ to account for the look-elsewhere effect.

While adjusting the estimated $P_{\rm cc}$ values is not necessary for the look-elsewhere effect owing to our use of a planned hypothesis testing framework in this study (for more information, refer to Anderson et al. 2001), it is worth noting that this perspective is widely challenged in the literature (see, e.g., Frane 2015). Hence, we proceed to adjust the estimated $P_{\rm cc}$ value for each of our FRBs to account for the look-elsewhere effect. To correct for the look-elsewhere effect, we use the Hochberg correction, also called Hochberg's step-up method (Hochberg 1988). It is an improvement over the Bonferroni correction employed by Bhardwaj et al. (2021a), as it provides increased statistical power, especially when the hypotheses being tested are either independent (which is true in our case) or positively correlated (Huang & Hsu 2007). The Hochberg correction limits the risk of inflating the overall Type I error rate (or false discovery rate) by adjusting the individual p-values for each hypothesis in a stepwise manner. To correct individual $P_{\rm cc}$ values, the Hochberg step-up procedure entails the following steps (for more detailed discussion, see Dunnett & Tamhane 1992):

Step 1: Arrange the estimated $P_{\rm cc}$ value for the four host associations in ascending order from smallest to largest.
Step 2: For each FRB host, calculate the adjusted $P_{\rm cc}$ value, or $P_{\rm cc,correct}$, using the following formula:

$$P_{\rm cc,correct} = \min((m - k + 1) \times P_{\rm cc}, 1), \quad (1)$$

where m is the total number of hypotheses being tested and k is the rank of the p-value in the ordered list. In our case, $m = 4$ and the $P_{\rm cc}$ value of FRB 20190425A being the smallest (3×10^{-4}) has rank 1, followed by those of FRB 20181220A ($k = 2$), FRB 20181223C ($k = 3$), and FRB 20190418A ($k = 4$).

Following the above procedure, we estimate the $P_{\rm cc,correct}$ values for all four FRBs as listed in Table 2. As the $P_{\rm cc,correct}$ values of all four low-DM CHIME FRBs in our sample are

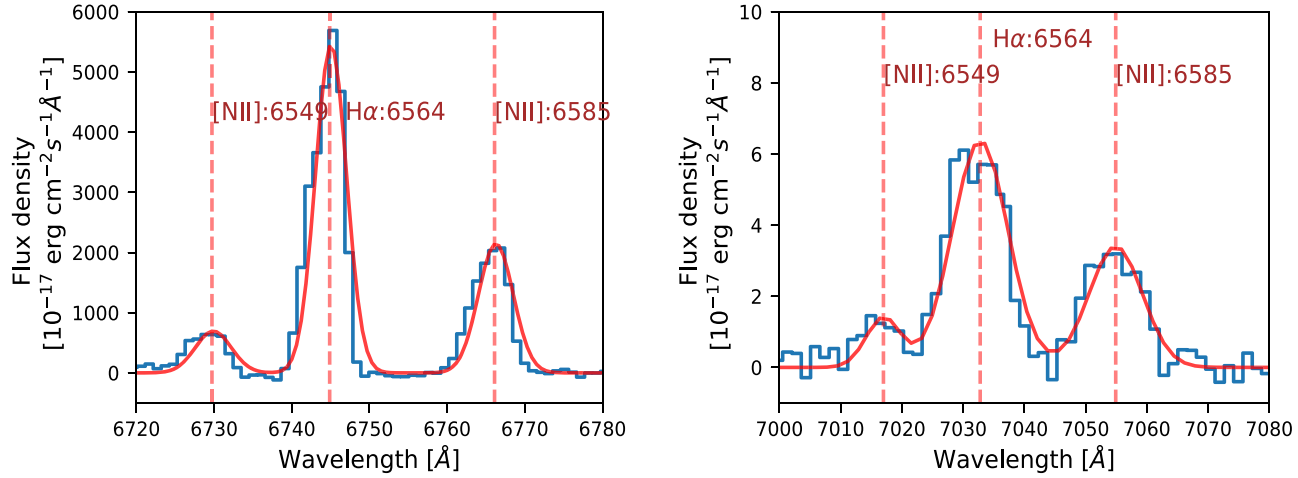

Figure 4. Galactic-extinction-corrected spectra (in the observer's frame) of the host galaxies for FRB 20181220A (left) and FRB 20190418A (right). The solid red lines depict the best-fitted line profiles estimated using `Specutils` for both galaxies, and the dotted vertical red lines denote the prominent nebular emission lines, Hα and [N II].

below the confidence threshold $(\alpha) = 0.1$ (as used in our planned hypothesis testing framework; see Section 2.1), it suggests that the identified host galaxy candidates are indeed likely host galaxies. Thus, along with the fact that we found only one plausible host candidate despite the fact that our search is sensitive to identifying hosts similar to or fainter than the faintest FRB host to the estimated maximum redshift of each FRB, we concluded that for all four FRBs the identified galaxies are indeed the most likely host galaxies.

There also exists a Bayesian framework to identify the host galaxies of FRBs, called PATH (Aggarwal et al. 2021). A Bayesian framework can address the problem of the look-elsewhere effect by relying on associated prior distributions, assuming that the priors accurately encapsulate the uncertainty surrounding the parameters being estimated (Sjolander & Vansteelandt 2019). However, the extent to which the prior distributions used in the PATH framework conform to the aforementioned requirement remains unclear. Once this is accessed robustly, PATH offers a promising alternative to the existing P_{cc} formalism. However, in the absence of such an assessment, we decide not to use this framework in our study. Nonetheless, when employing PATH with its default priors, except for an undetected host prior $P(U) = 0.1$, the $P(O|x)$ for each FRB to the suggested host galaxy exceeds 0.90, supporting the results of the preceding analysis.

2.4. Host Galaxy Properties

To estimate major physical properties of the host galaxies of the four low-DM FRBs, we use a Bayesian inference spectral energy distribution (SED) fitting code, `Prospector` (Leja et al. 2017; Johnson et al. 2019). Appendix A describes the SED fitting analysis in detail. Major host properties of the four FRBs are presented in Table 2.

2.5. Multiwavelength Counterpart Searches

We search for any promising association of the four low-DM FRBs with transients, such as SNe, gamma-ray bursts, active galactic nucleus (AGN) flares, and gravitational-wave (GW) events, which are proposed to be plausible sources for at least some apparently nonrepeating FRBs. We first search the

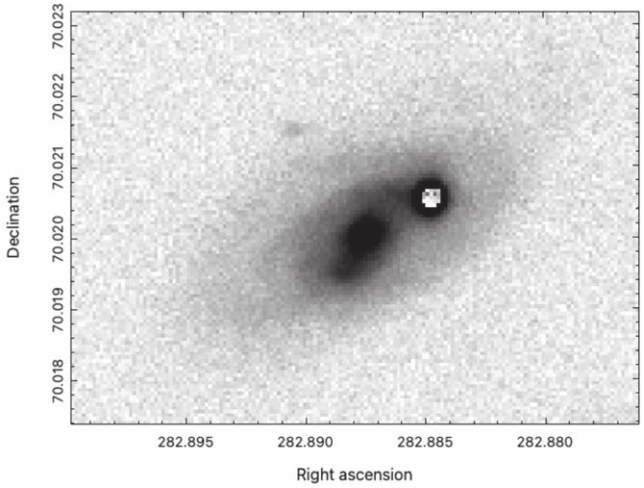

Figure 5. The CFIS DR3 r-band image of the FRB 20220509G host (in ICRS reference frame). The star in close proximity to the FRB host is flagged for better visualization of the extended spiral arm features.

Transient Name Server[31] (TNS) database (Yaron et al. 2020) for transients (both classified and unclassified) up to 2023 August 1 for transients within the 2σ baseband localization region of the four FRBs, and we find none. We note that FRB 20190425A is proposed to be possibly associated with the GW190425 event, which we discuss in Section 2.5.2. We next search the Zwicky Transient Facility (Graham et al. 2019) public alert stream for transient candidates within the baseband localization of FRBs to check for any possible missed transients that are not reported to the TNS or are not classified there. Again, we find none. From this, we conclude that the four low-DM apparently nonrepeating FRBs are unlikely to be temporally and spatially associated with any SNe, any GRBs, and most luminous AGN flares ($>10^{45}$ erg; Pietka et al. 2015) reported in the two databases. We now discuss our search for the presence of any persistent compact radio source, as these are found to be spatially colocated with at least two FRB sources (Chatterjee et al. 2017; Niu et al. 2022).

[31] http://www.wis-tns.org

Table 2
Major Observables of the CHIME FRB Hosts

Parameter	FRB 20181220A	FRB 20181223C	FRB 20190418A	FRB 20190425A
R.A. (J2000)[a] (deg)	348.6982	180.9207	65.8123	255.6625
Decl. (J2000)[a] (deg)	48.3421	27.5476	16.0738	21.5767
Galaxy name	2MFGC 17440	SDSS J120340.98+273251.4	SDSS J042314.96+160425.6	UGC 10667
Apparent r-band mag (m_r; AB)	15.71	16.78	16.68	14.77
Galactic r-band extinction (A_r; AB)	0.45	0.05	1.28	0.17
P_{cc}	0.01	0.02	0.08	3×10^{-4}
$P_{cc,corrected}$ [b]	0.03	0.04	0.08	1.2×10^{-3}
Spectroscopic redshift (z_{spec})	0.02746 ± 0.00003	0.03024 ± 0.00001	0.07132 ± 0.00001	$0.03122 \pm \pm 0.00001$
Absolute r-band mag (M_r; AB)	-19.71	-18.85	-20.95	-20.93
Effective radius, R_{eff} (kpc)[c]	5.2	2.1	3.7	4.6
SFR (Hα; $M_\odot$ yr^{-1})[d]	3.0 ± 0.3[e]	0.054 ± 0.002[f]	0.15 ± 0.04[e]	1.5 ± 0.5[g]
SFR (0−100 Myr; $M_\odot$ yr^{-1})[h]	$2.9^{+1.6}_{-0.9}$	$0.15^{+0.12}_{-0.08}$	$0.8^{+1.1}_{-0.6}$	$1.6^{+1.5}_{-0.9}$
Stellar mass $\log(M/M_\odot)$[h]	$9.86^{+0.14}_{-0.12}$	$9.29^{+0.16}_{-0.20}$	$10.27^{+0.13}_{-0.17}$	$10.26^{0.09}_{-0.1}$
Stellar metallicity $\log(Z/Z_\odot)$[h]	$-0.03^{+0.24}_{-0.18}$	$-0.7^{+0.4}_{-0.5}$	$-1.51^{+0.47}_{-0.35}$	$-0.6^{+0.4}_{-0.5}$
Mass-weighted age (Gyr)[h]	$2.7^{+2.4}_{-1.6}$	$6.6^{+0.2}_{-2.1}$	$5.5^{+2.1}_{-2.5}$	$6.8^{+2.0}_{-2.3}$
Log(specific SFR$_{0-100\ Myr}$; yr^{-1})[h]	$-9.4^{+0.2}_{-0.2}$	$-9.75^{+0.26}_{-0.33}$	$-10.35^{+0.42}_{-0.71}$	$-10.20^{+0.36}_{-0.43}$
A_V[h]	$0.79^{+0.20}_{-0.18}$	$0.16^{+0.07}_{-0.05}$	$0.21^{+013}_{-0.09}$	$0.66^{+0.16}_{-0.18}$
Host AGN[h]	N	N	N	N
PRS luminosity (3σ u.l.; 10^{37} erg s^{-1})	3.3	4.0	23.8	4.3
Inclination angle (deg)	75 ± 1[i]	36 ± 5[j]	61 ± 3[i]	69 ± 1[j]

Notes.
[a] Centroid coordinate of the host galaxy.
[b] P_{cc} corrected for the look-elsewhere effect using the formalism discussed in Section 2.3.
[c] Half-light radius values of all except FRB 20181220A host are estimated using SDSS catalog r-band Petrosian magnitudes (Abdurro'uf et al. 2022) and Equation (7) of Graham et al. (2005). The half-light radius of the FRB 20181220A host is estimated using the `Petrofit` package (Geda et al. 2022).
[d] Values obtained using the optical spectrum of the host galaxies.
[e] To correct for host extinction, we use $E(B-V) = A_v/R_v = 0.19$ and 0.06 for FRB 20181220A and FRB 20190418A, respectively. These values are estimated using `prospector`. For fair comparison with the `Prospector` SFR estimates, we use the SFR−Hα relation from Kennicutt (1998), but adopting the IMF from Chabrier (2003): SFR($M_\odot$ y^{-1}) $= 4.98 \times 10^{-42}$ $L_{H\alpha}$ (erg s^{-1}).
[f] From Panther et al. (2023).
[g] From Duarte Puertas et al. (2022).
[h] Estimated using `Prospector`.
[i] The inclination angle is estimated using the `IncliNET` package (Kourkchi et al. 2020).
[j] From Simard et al. (2011).

2.5.1. Persistent Radio Source Search

We search archival radio data from the following catalogs to check for the presence of a persistent radio source within the four FRB baseband localization regions: the NRAO VLA Sky Survey (NVSS; Condon et al. 1998), Faint Images of the Radio Sky at Twenty cm (FIRST) survey (Becker et al. 1995), the VLA Sky Survey (VLASS; Lacy et al. 2016), the Rapid ASKAP Continuum Survey Data Release 1 (RACS DR1; Hale et al. 2021), the Westerbork Northern Sky Survey (WENSS; Rengelink et al. 1997), the Tata Institute of Fundamental Research Giant Metrewave Radio Telescope Sky Survey Alternative Data Release (TGSS; Intema et al. 2017), and the Low-Frequency ARray (LOFAR) Two-meter Sky Survey Data Release 2 (LoTSS DR2; Shimwell et al. 2022). The results of our archival search are presented in Table 3. As can be inferred from the table, only in the case of FRB 20181220A do we find an extended radio source, NVSS J231448+482039, with an integrated flux density of 2.4 ± 0.4 mJy. The radio source is only detected in NVSS. Moreover, it is spatially coincident with the center of the host galaxy of FRB 20181220A, 2MFGC 17440. The NVSS source is likely due to ongoing star formation in 2MFGC 17440. To test this, we estimate the SFR of the FRB host using the following radio–SFR relation from Murphy et al. (2011): $\log(\mathrm{SFR}_{H\alpha}/M_\odot\,\mathrm{yr}^{-1}) = \log(L_{1.4}(\mathrm{W\,Hz}^{-1})) - 21.20 = 0.45$, i.e., $2.8\,M_\odot\,\mathrm{yr}^{-1}$, which matches with the $\mathrm{SFR}_{H\alpha}$ value reported in Table 2. Hence, the observed 1.4 GHz radio emission in the FRB 20181220A host is likely due to ongoing star formation in the host.

Based on this analysis, we find no credible persistent compact radio source within the 2σ localization regions of the four low-DM FRBs. To estimate an upper limit on the isotropic luminosity of a putative compact radio source, we use VLASS 2.1 data owing to its superior angular resolution ($2\farcs5$) among the radio surveys considered in this study. This enables us to derive a 3σ upper limit on the luminosity of any potential compact radio source at 3 GHz, as stated in Table 2. For all four FRBs, we rule out a persistent radio source like the one found to be spatially coincident with the FRB 20121102A and FRB 20190520B sources ($\approx 7 \times 10^{38}$ erg s^{-1} at 3 GHz; Chatterjee et al. 2017; Resmi et al. 2021; Niu et al. 2022).

2.5.2. Proposed Association between FRB 20190425A and GW190425

The LIGO Scientific Collaboration et al. (2023) searched for GW transients associated with FRBs detected by the CHIME/FRB project, during the first part of the third observing run of Advanced LIGO and Advanced Virgo (2019 April 1 15:00 UTC–2019 October 1 15:00 UTC). This duration includes two

Table 3
Summary of the Radio Limits for the Four FRBs Derived Using Archival Surveys

FRB Name[a]	LoTSS DR2	TGSS	WENSS	RACS DR1	NVSS	FIRST	VLASS
20181220A	⋯	<10.5 mJy	<10.8 mJy	⋯	2.4 ± 0.4 mJy	⋯	<0.48 mJy
20181223C	<0.250 mJy	<10.5 mJy	⋯	<3 mJy	<1.3 mJy	<0.45 mJy	<0.48 mJy
20190418A	⋯	<10.5 mJy	⋯	<3 mJy	<1.3 mJy	⋯	<0.48 mJy
20190425A	⋯	<10.5 mJy	⋯	<3 mJy	<1.3 mJy	<0.45 mJy	<0.48 mJy
Frequency[b] (GHz)	0.144	0.150	0.326	0.888	1.4	1.5	3

Notes.
[a] For each survey, if the FRB localization region is covered but no source has been detected, a flux density upper limit of 3× local rms noise is used. In addition, ellipsis points are used to indicate that the survey does not cover the FRB localization region.
[b] Central frequency of a given survey.

Table 4
Sample of 18 Local Universe FRBs ($z_{\rm host} \leqslant 0.1$) Considered in This Study

FRB	Galaxy Morphology	Redshift	Repeater (Y/N)	References
20200120E	Spiral	−0.0001[a]	Y	Bhardwaj et al. (2021a)
20181030A	Spiral	0.0039	Y	Bhardwaj et al. (2021b)
20171020A	Spiral	0.0086	N	Mahony et al. (2018) Lee-Waddell et al. (2023)
20220319D	Spiral	0.011	N	Ravi et al. (2023b)
20181220A	Spiral	0.0275	N	This work
20181223C	Spiral	0.0302	N	This work
20190425A	Spiral	0.0312	N	This work
20180916B	Spiral	0.0337	Y	Marcote et al. (2020)
20220207C	Disk-dominated	0.043	N	Law et al. (2024)
20211127I	Spiral	0.0469	N	Gordon et al. (2023) Glowacki et al. (2023)
20200223B	Spiral	0.0602	Y	Ibik et al. (2024)
20190303A	Spiral	0.064	Y	Michilli et al. (2023)
20210405I	Spiral	0.066	N	Driessen et al. (2024)
20190418A	Spiral	0.0715	N	This work
20211212A	Spiral	0.0715	N	Gordon et al. (2023)
20220912A	Disk-dominated	0.077	Y	Ravi et al. (2023a)
20220509G	Spiral (Figure 5)	0.0894	N	This work (see Appendix D)
20201124A	Spiral	0.098	Y	Xu et al. (2022)

Note.
[a] The line-of-sight velocity of M81 is dominated by its peculiar velocity. The comoving distance of M81 from us is ≈3.6 Mpc (Buta 2019).

low-DM FRBs whose host galaxies are reported in this Letter. Although the authors found no significant evidence for a GW association (for time delay $\sim \pm$ few seconds) in their search, Moroianu et al. (2023) reported a possible association, at the 2.8σ level, between GW190425 (Abbott et al. 2020), the second binary neutron star (BNS) merger to be detected in GW, and FRB 20190425A, with UGC 10667 as the most probable host galaxy (Panther et al. 2023). Nonetheless, Bhardwaj et al. (2023) reevaluated the association, taking into account the effect of highly dense and turbulent BNS ejecta, as well as the expected off-axis nature of the merger if these events are related. Their findings suggest that the two events are very likely unrelated.

3. Discussion

3.1. Host Demographic Analysis

We now utilize the four FRB host galaxies reported in this work to explore the demographics of the FRB host population. Our aim is to derive meaningful constraints on the potential formation channels of FRBs. To broaden the scope of our investigation, we have incorporated all published and robustly associated FRB host galaxies to $z = 0.1$, which we will henceforth refer to as the "local Universe FRB host sample." This specific redshift cutoff is based on our DM excess $\leqslant 100\,{\rm pc\,cm^{-3}}$ constraint, which effectively narrows down our FRB host search to within $z \approx 0.1$, as discussed in Section 2.1. As of 2023 July, we found 18 published FRBs in the literature with robustly associated host galaxies ($P_{\rm cc} \leqslant 10\%$, or a $P(O|x) > 90\%$) located within $z = 0.1$. These are presented in Table 4. Additionally, there is no observed statistically significant distinction between the hosts of repeating and apparently nonrepeating FRBs based on any of their major modeled physical properties (Gordon et al. 2023). This suggests that they arise from the same progenitors, or from multiple progenitors that form and evolve in similar environments. Therefore, we do not make any distinction between them in the subsequent analysis, except in Section 3.1.3.

We acknowledge that our local Universe FRB sample comprises hosts localized by different telescopes, each with its own distinct selection effects. Consequently, the sample may exhibit unmodeled biases, potentially impacting the statistical analyses presented in the following sections. To address these concerns, we have undertaken the approach of performing only those analyses where either the selection bias is not important

or its inclusion would only strengthen our conclusions. By doing so, we aim to mitigate the impact of potential biases and ensure the robustness of our findings.

For example, about 33% of the FRBs in our local Universe FRB host sample were detected using the DM excess $\leqslant 100\,\mathrm{pc\,cm^{-3}}$ constraint employed in this work. This particular constraint tends to favor FRBs in which the host's DM contribution is relatively low. Additionally, it should be noted that early-type galaxies, on average, would likely contribute less DM to the FRB host than late-type galaxies, such as spirals (Xu & Han 2015; Chawla et al. 2022). Moreover, the interstellar medium in spiral galaxies likely contributes more to scattering than in early-type galaxies (Chawla et al. 2022). This may impact the detectability of FRBs in late-type host galaxies, particularly if a substantial number of FRBs originate from star-forming regions within the thin disk (Ocker et al. 2022; Bhardwaj et al. 2024). Therefore, the low DM excess constraint would introduce a bias against detecting FRBs in spiral galaxies. Hence, if we detect more spiral hosts, the significance of this observation would only be strengthened by including the selection bias stemming from the low DM excess cutoff. Furthermore, we note that the low DM excess cutoff can also introduce a bias against detecting FRBs in galaxies residing in massive halos ($>10^{12}\,M_{\odot}$), including galaxy clusters and groups, if their halos can contribute significantly to the observed host DMs. However, it is unclear how significant this bias would be. For instance, in a study conducted by Khrykin et al. (2024) using the SIMBA suite of simulations, it was demonstrated that various feedback processes, including AGN-driven jets, can result in the loss of more than 50% of the CGM mass from such massive halos into the intergalactic medium. Even if such a bias against massive halos due to the low DM excess cutoff were to exist, it seems improbable that it would result in an overrepresentation of late-type hosts in comparison to early-type hosts. To illustrate, untargeted surveys conducted with radio telescopes, such as the Australian Square Kilometre Array Pathfinder (ASKAP; Shannon et al. 2018) and the Deep Synoptic Array-110 (DSA-110; Ravi et al. 2023a), which do not impose a low DM excess cutoff, have collectively identified over 30 FRB hosts to date (Gordon et al. 2023; Law et al. 2024). However, these surveys have not yet detected any FRBs associated with massive elliptical hosts, while multiple massive late-type hosts have been identified.

3.1.1. Prevalence of Local Universe FRBs in Spiral/Late-type Galaxies

To broadly determine and utilize the FRB host population using the local Universe FRB sample, we first identify the morphological class of FRB host galaxies in our sample. Using the widely accepted formalism in the literature (Buta 2011), we define two morphological classes: (1) early-type galaxies, i.e., ellipticals (E), and transition E/S0 galaxies, which include those centrally concentrated galaxies that look spheroidal or ellipsoidal with a regular shape and no or weak hints of a disk morphology (in short, single-component bulge-dominated galaxies; Kelvin et al. 2014); and (2) late-type galaxies, i.e., spirals (S), irregulars (Irr), and merging galaxies, i.e., galaxies with a clear disk and/or irregular structure or S or Irr with a hint of an ongoing merger process.

In Section 2.2, we noted that all four low-DM FRB hosts reported in this work are spiral or disk-dominated galaxies based on their morphologies. For the remaining 14 local Universe FRB hosts, we look for existing morphological classification in the NED and SIMBAD databases, and we find that the following eight local Universe FRB hosts are classified as "spiral" based on their morphology: FRB 20171020A, FRB 20180916B, FRB 2081030A, FRB 20190303A, FRB 20200120E, FRB 20200223B, FRB 20220207C, and FRB 20220319D.

Next, we examine the host morphology of the remaining six local Universe FRB host galaxies for the clear presence of the well-formed disk, spiral arms, or bar features in available public images of the FRB hosts. Except for FRB 20220509G, we find that the remaining five FRB host galaxies in our sample, FRB 20201124A, FRB 20210405I, FRB 20211127I, FRB 20211212A, and FRB 20220912A, show either a well-formed disk, spiral arms, or barlike morphology, as noted by the authors in their respective discovery papers as referenced in Table 4. For a detailed discussion on this, see Appendix C.

We note that FRB 20220509G is classified as elliptical by the authors in their discovery papers (Connor et al. 2023; Sharma et al. 2023). However, we find a clear presence of barlike structure and disk morphology in the Canada–France Imaging Survey (CFIS) *r*-band image as shown in Figure 5 (Ibata et al. 2017; Fantin et al. 2019), which is at least 3 mag deeper than the Pan-STARRS image used by Sharma et al. (2023). For more discussion on this, see Appendix D. Therefore, we conclude that the FRB 20220509 host is a spiral galaxy.

Additionally, we look at the Wide-field Infrared Survey Explorer (WISE) color–color classification for the morphological classification of the FRB hosts. We find that all 18 FRB host galaxies are detected in WISE and are classified as spirals or star-forming disk galaxies based on the WISE color–color plot shown in Figure 6 (Wright et al. 2010). For this analysis, we use the AllWISE full-sky data release (Cutri et al. 2021) and extended source (Jarrett et al. 2020) catalogs to estimate WISE W1 (3.4 μm) − W2 (4.6 μm) and W2 (4.6 μm) − W3 (12 μm) colors of the 18 local Universe FRB hosts listed in Table 4. Overlaid on the same plot are classification thresholds, as estimated by Jarrett et al. (2017), to separate early-type (spheroidal), intermediate-type (disk), and late-type (star-forming disk) galaxies. Note that the only FRB host consistent with a spheroid/old disk classification according to Jarrett et al. (2017) is M81, which is a grand-design spiral galaxy. The figure clearly reveals that all 18 FRB host galaxies occupy the WISE color–color phase space associated with spiral galaxies or are located within the star-forming disk region. This observation, in conjunction with the morphological evidence discussed earlier, solidifies the classification of all 18 FRB hosts as spiral or late-type galaxies.

The presence of 18 FRB sources in spiral hosts is an intriguing observation, as our local Universe host sample is likely biased against spirals (see Section 3.1). We next examine whether the distribution of FRB hosts aligns with the expected number of spirals in the local Universe (∼70%−80%; Delgado-Serrano et al. 2010; Deng 2013; Hart et al. 2016; Grootes et al. 2017). Using binomial statistics, we test this hypothesis and find a 1.8% likelihood of this outcome by chance assuming the local Universe spiral fraction = 80%. Therefore, the notable excess of spirals among FRB hosts is noteworthy, suggesting a strong preference for FRB sources within spiral or late-type galaxies.

Note that the observed prevalence of late-type FRB host galaxies within the local Universe holds the potential to constrain the age of FRB progenitors. This is demonstrated by

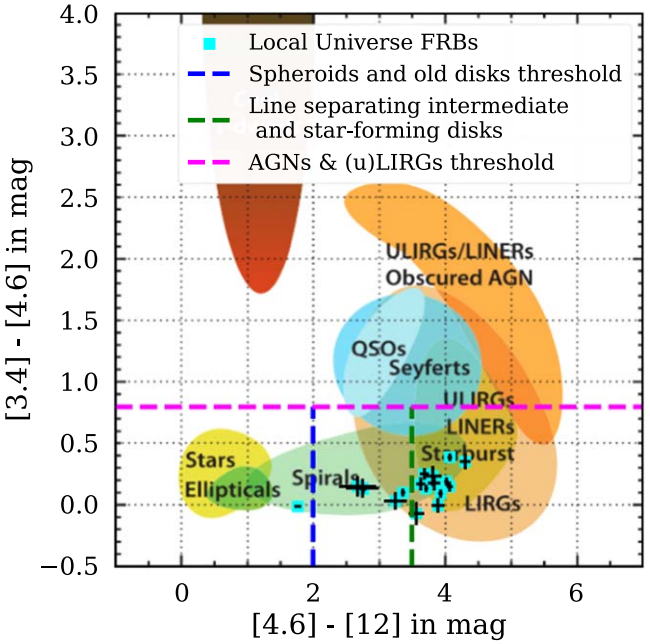

Figure 6. WISE color–color plot adapted from Wright et al. (2010) for our sample of local Universe FRB hosts. It illustrates how galaxies separate by type, showing the simple divisions for spheroidal and early-type disks, intermediate disks, and late-type disk galaxies (Jarrett et al. 2017). The infrared colors of all 18 local Universe FRB hosts support them being spiral or late-type galaxies. For a detailed description of each shaded region, kindly refer to Wright et al. (2010).

the distinction between early- and late-type galaxies, where the former generally exhibit earlier star formation than the latter. Consequently, the stellar populations in early-type galaxies tend to be older than those in their late-type counterparts (Muzzin et al. 2013; Scott et al. 2017). This distinction in the average ages of the stellar populations, coupled with the inherent time delay between the peak star formation in the host galaxies (assuming that the FRB progenitors are most likely to form during that period) and FRB occurrences, ultimately gives rise to discernible event rates between these two host categories. Such studies have been conducted for short GRBs (sGRBs), in which the probability distribution of the time delay for sGRB progenitors is assumed to follow a power law with an index n, such that $P(\tau) \propto \tau^n$ (Zheng & Ramirez-Ruiz 2007). If we employ this formalism for FRB progenitors using the early-to-late-type host ratio $\sim$0.06, we would constrain the power-law index for the FRB progenitors to be $n < -1.5$ (from Figures 2 and 4 of Zheng & Ramirez-Ruiz 2007), a value steeper than what is observed for Type Ia SNe (SNe Ia; $n \approx -1$). Note that a steeper power-law index indicates that the majority of FRB progenitors exhibit shorter time delays (or lower ages for the progenitors of FRB sources) in comparison to the progenitors of SNe Ia. We further elaborate on this in the following section.

3.1.2. What Is Likely the Dominant FRB Formation Channel?

The observed preponderance of local Universe FRBs in spirals or late-type galaxies bears an important clue about their dominant source formation channels. This preponderance might also extend to higher redshifts, as no elliptical FRB host has been reported to date even at $z > 0.1$. In this section, based on the observed excess of spiral host galaxies, we aim to identify the dominant FRB formation channel. However, we note that this does not exclude the possibility that a small fraction of FRBs might be produced by channels other than the dominant one.

CCSN formation channel: This channel, encompassing Type Ib SNe (SNe Ib), Type Ic SNe (SNe Ic), and Type II SNe (SNe II), is mostly observed in star-forming late-type galaxies, as noted in various studies (e.g., Svensson et al. 2010; Kelly & Kirshner 2012; Perley et al. 2020; Schulze et al. 2021). This can be attributed to their likely origin from the collapse of massive stars ($\geqslant 8\,M_{\odot}$). Considering that the lifetimes of these stars are expected to be shorter than 150 million years (Zapartas et al. 2017), CCSNe should predominantly emerge in galaxies that are either young or actively undergoing star formation. These categories primarily encompass spiral galaxies but also include irregular galaxies, providing a natural explanation for the observed prevalence of spiral hosts for local FRBs. Furthermore, observables such as host offsets, SFR, and stellar mass, derived from the existing albeit small sample of FRB host galaxies, align with the characteristics expected for neutron stars formed via prompt channels (Li & Zhang 2020; Bochenek et al. 2021; Chrimes et al. 2021).

However, there exist observations that potentially challenge this assertion, for instance, the detection of FRB 20200120E in an M81 GC (Bhardwaj et al. 2021a; Kirsten et al. 2022) and the linkage of FRB 20180814A (a repeating FRB; Michilli et al. 2023) and FRB 20220509G (an apparently nonrepeating FRB; Sharma et al. 2023) to quiescent spiral galaxies. We delve into these specific cases below. In the subsequent paragraphs, we explore whether alternative formation channels could also account for the excess of late-type FRB hosts within the local Universe.

Long GRBs (LGRBs) and superluminous SN (SLSN) formation channel: These channels have been proposed to form potential sources for repeating FRBs, exemplified by FRB 20121102A (Metzger et al. 2017). The formation channels are invoked to account for distinct features in the case of FRB 20121102A, including the presence of a low-metallicity dwarf host, a persistent radio source, and heightened activity in the repeating FRB source potentially linked to its young age (Nicholl et al. 2017). However, subsequent analyses of FRB host properties, such as the distribution of offsets between hosts and bursts, host stellar mass, and metallicity, seem inconsistent with LGRBs and SLSNe as the prevailing channels for FRB source formation (Bhandari et al. 2020, 2022). Furthermore, the high volumetric rate of local Universe FRBs cannot be explained by the proposed formation of millisecond magnetars through these channels (Bhardwaj et al. 2021b). Therefore, despite their occurrence in late-type star-forming galaxies (mostly dwarfs), we argue against LGRBs and SLSNe as the dominant FRB source formation channels.

GC origin of FRB sources: The discovery of FRB 20200120E within an old M81 GC suggests the potential for dynamically formed FRB sources within dense cluster cores, potentially via the accretion-induced collapse of white dwarfs and binary white dwarf mergers (Kirsten et al. 2022; Kremer et al. 2021a). It is now widely acknowledged that the populations of GCs in galaxies correlate with the stellar and dark halo mass of their host galaxies (Hudson et al. 2014). This suggests that if GCs are the principal sources of FRBs, the overall FRB rate should primarily follow stellar mass. In this scenario, the relative detection rates of FRBs in early- and late-type FRB host galaxies should align with the distribution of

stellar mass in these galaxies. Kelvin et al. (2014) analyzed a morphologically classified sample of 2711 local Universe galaxies ($z < 0.1$) selected from the Galaxy and Mass Assembly (GAMA) survey with global stellar mass (($\log(M_*/M_\odot > 9.0$) and found that ≈71% of the stellar mass in the local Universe is currently found within early-type galaxies (elliptical and S0–Sa). However, our local Universe FRB host sample does not have any early-type hosts (including unbarred quiescent spiral with dominant central bulge, Sa; Whyte et al. 2002). Using binomial statistics, we find that the probability of finding no early-type host in our sample strongly disfavors (p-value ≈ 0) the null hypothesis that FRBs trace stellar mass alone. This remains true even when we consider only those local Universe FRB hosts in our sample that were not identified using the low DM excess cutoff (i.e., 12 hosts). Therefore, we conclude that GC sources are not the dominant formation channel of FRBs.

Delayed formation channels linked with SNe Ia: Several delayed formation pathways for FRB sources have been proposed, including binary white dwarf mergers (Piro & Kulkarni 2013; Liu 2018; Zhao et al. 2021) and accretion-induced collapse of white dwarfs (Zhong & Dai 2020; Kremer et al. 2023). These scenarios are theorized to either lead to SNe Ia or share comparable rates and local environments to SNe Ia (Fryer et al. 1999; Hillebrandt & Niemeyer 2000; Ruiter et al. 2010; Kashiyama et al. 2013). Hence, in this section we consider SNe Ia as representative of these models. It is important to note that in this context the cataclysmic channels mentioned earlier do not take place within GCs and, consequently, they are not anticipated to solely follow the distribution of stellar mass (Kremer et al. 2021b). However, unlike CCSNe, SNe Ia originate in a mix of early- and late-type galaxies (Pan et al. 2014). To assess whether SNe Ia explain the observed late-type galaxy fraction, we analyze late-type SN Ia host galaxies ($z \leqslant 0.1$) using the Pantheon cosmological SN catalog (Scolnic et al. 2018), yielding a fraction of 0.76. For a detailed discussion, see Appendix E. Employing binomial statistics, we test the null hypothesis of an inherent fraction of the late-type hosts of 0.76. The observed late-type FRB host fraction of 1 results in a p-value of 0.007, hence disfavoring the null hypothesis. Thus, FRB formation channels that trace SNe Ia appear unlikely to be the dominant FRB source formation channel.

Delayed formation channels linked to BNS mergers: BNS mergers have been proposed as possible FRB source formation channels (Totani 2013; Falcke & Rezzolla 2014; Most et al. 2018; The LIGO Scientific Collaboration et al. 2023). Moreover, alongside neutron star–black hole mergers, they are also believed to produce sGRBs (Sarin et al. 2022). While the similarity in the offset distribution of FRBs and sGRBs from their host nuclei is noteworthy (Heintz et al. 2020; Bhandari et al. 2022), sGRBs, like SNe Ia, are observed in both early- and late-type galaxies, differing from what we found in our local Universe FRB host sample (Fong et al. 2022; O'Connor et al. 2022). Moreover, BNS mergers struggle to explain the high all-sky FRB rate ($\{525 \pm 30\}^{+142}_{-131}$ FRBs sky^{-1} day^{-1}; CHIME/FRB Collaboration et al. 2021) even if most of their remnants become repeating FRBs (Zhang et al. 2020; Bhardwaj et al. 2023). Therefore, BNS mergers are unlikely to be the dominant formation channel of FRB sources.

After examining all major FRB source formation channels studied in the literature, we argue that CCSNe are the only channel that can explain the observed excess of late-type galaxies in the local Universe FRB host sample along with other FRB observables. Therefore, we argue that CCSNe are likely the dominant FRB source formation channel. In Appendix F, we discuss whether the FRB host population in the local Universe is consistent with that of CCSNe.

3.1.3. Comparison of the Host Properties of Repeating and Apparently Nonrepeating FRBs

The vast majority of FRB sources have only been detected once, but a small subpopulation ($\lesssim$3%) is known to burst repeatedly (CHIME/FRB Collaboration et al. 2021, 2023). This naturally raises speculations that there are two distinct classes of FRBs (Caleb et al. 2018, 2019; Palaniswamy et al. 2018). Supporting evidence comes from the strong temporal and spectral differences (including in the DM distribution) of repeater and apparent nonrepeater bursts (Pleunis et al. 2021). In terms of FRB energetics, we also find that repeating FRBs are capable of producing bursts of energy comparable to what is seen for apparently nonrepeating localized FRBs (Ould-Boukattine et al. 2022; Kirsten et al. 2024). Given that all other major observables of the two classes remain statistically indistinguishable for the two populations (CHIME/FRB Collaboration et al. 2021; Cui et al. 2021; Zhang et al. 2022), it is not unreasonable to assume that they have a common origin (see, e.g., James 2023). A similar inference can be made by comparing their host galaxies. For example, Bhandari et al. (2022) and Gordon et al. (2023) found the global properties of repeating and apparently nonrepeating FRB hosts to be statistically indistinguishable. However, it is important to note that the sample size of FRB hosts employed in their study may not be large enough to ensure the robustness of the inferred conclusions. For example, Gordon et al. (2023) note that the hosts of repeating FRBs generally extend to lower stellar masses and that the hosts of nonrepeating FRBs arise in more optically luminous galaxies. But for our local Universe FRB sample, as can be inferred from Figure 13 in Appendix F, the median masses of repeating and apparently nonrepeating FRB hosts are comparable ($\log(M/M_\odot) = 10.1$ and 10.2, respectively). However, we note that the median absolute r-band magnitude (M_r) of apparently nonrepeating FRB hosts is ≈1 AB mag larger than that of repeating FRBs, which was also noted by Gordon et al. (2023). Moreover, in their sample of 23 FRBs, consisting of 6 repeating FRBs and 17 apparently nonrepeating FRBs, Gordon et al. (2023) found that four out of six repeating FRB hosts show peaks in their SFRs within a look-back time of 100 Myr (often called time delay), while for the apparently nonrepeating FRBs that ratio is only 7 out of 17. Assuming that the FRB progenitor (zero-age main-sequence (MS) star) was born at the time of peak star formation, this might imply that repeating FRB sources are statistically younger than apparently nonrepeating ones, as a more active central engine should correspond to a younger age. Using Prospector and a nonparametric star formation history (SFH), we show in Figure 7 the SFHs of the four low-DM FRB host galaxies reported in this study over look-back time, which is estimated using the formalism discussed in Appendix A. For the four low-DM FRBs, we find that three FRBs show time delays $\lesssim$100 Myr, as can be inferred from Figure 7, which is at odds with the aforementioned observation made by Gordon et al. (2023). Thus, we clearly need a larger sample of both repeating and apparently nonrepeating FRB hosts to truly see any statistical difference between the distributions of their delay times.

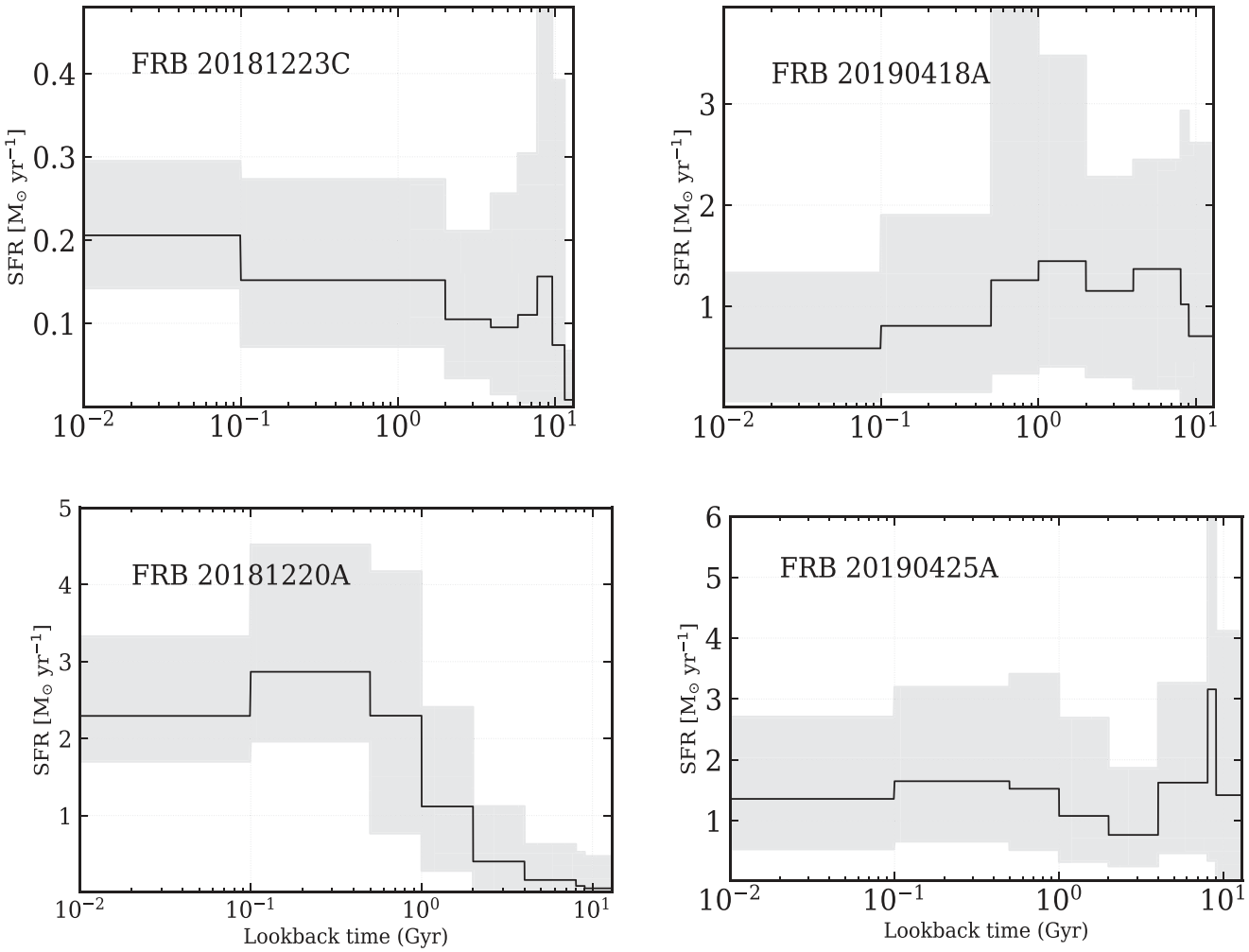

Figure 7. SFHs of the four FRB host galaxies reported in this work. The *x*-axis is the look-back time (Gyr), such that the left panel shows the present day and the right panel shows the age of the Universe at the redshift of the galaxy. These SFHs are estimated using `Prospector`. For more details, see Appendix A.

3.2. Are All Local Universe FRBs Repeating Sources?

Based on the high volumetric rate of local Universe CHIME bursts, Bhardwaj et al. (2021b) argued that the nearby CHIME FRBs are likely to be repeating sources. Therefore, we searched for repeat bursts from the four low-DM FRBs in CHIME data at epochs between 2019 September 30 and 2021 May 1, using the formalism employed by CHIME/FRB Collaboration et al. (2023), and found none. Briefly, we first calculate the effective Poisson burst rates of the four apparently nonrepeating FRBs based on the effective exposure time within the baseband localization region (3σ) of the FRBs and sensitivity (using fluence threshold of 5 Jy ms, i.e., the average sensitivity of the CHIME/FRB system; Josephy et al. 2021) and on the detection of one burst from each source. We then infer 68% confidence intervals on each rate using the Kraft et al. (1991) formalism. Note that we estimate the total on-sky exposure only for the upper transit (more sensitive) for the FRBs from the start of the experiment, 2018 August 28, through to 2021 May 1 from the CHIME/FRB exposure map produced and made public by CHIME/FRB Collaboration et al. (2023). The exposure values of the four FRBs are stated in Table 1. To remove the effect of cosmological-distance-related selection effects that can bias against detecting repeat bursts from more distant FRBs, we compare the distance-independent burst rates of the four low-DM FRBs with those of well-localized repeating FRBs that either have been discovered or have had at least one burst detected by CHIME (in the case of FRB 20121102A). We first convert the fluence sensitivity threshold for each FRB in this study into respective isotropic energies using the host redshifts reported in the discovery papers. For CHIME/FRB repeating sources such as FRB 20200223B, FRB 20190110C, FRB 20180814A, FRB 20180916B, FRB 20181030A, FRB 20190303A, and FRB 20201124A, the burst rates at 5 Jy ms have been already reported by CHIME/FRB Collaboration et al. (2023). For FRB 20121102A, we use the fluence sensitivity threshold of 7 Jy ms from Josephy et al. (2019) and $z = 0.19273$ from Tendulkar et al. (2017). We then scale the burst rates to the fiducial FRB isotropic energy threshold of 10^{39} erg s^{-1}.

The scaling involves the assumption of a power-law index of -1.5 for the cumulative burst energy distribution of each source, as assumed by CHIME/FRB Collaboration et al. (2023). Figure 8 shows the scaled burst rate of the localized repeating sources and the four apparently nonrepeating sources, respectively. As shown in the plot, although the burst rates of the four low-DM FRBs are lower than those of localized CHIME repeating sources, they are still larger than the observed burst rates of FRB 20181030A. This suggests that there is a large variation in the burst rates of localized repeating sources, and thus it is still possible for the four

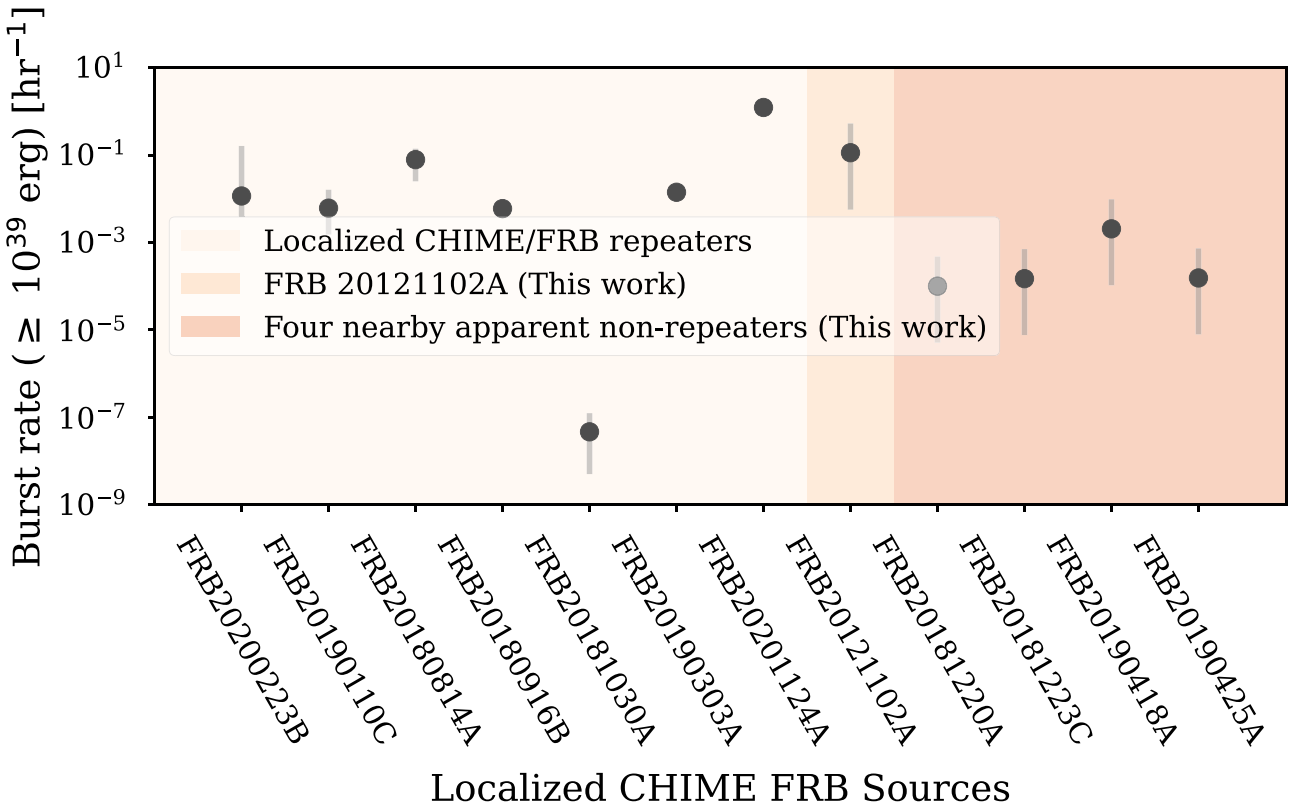

Figure 8. Comparison of the effective Poisson burst rates of the four low-DM FRBs studied in this work with those of published CHIME/FRB repeating sources with known hosts.

low-DM FRBs to be repeating sources. Therefore, we encourage further follow-up of these sources using more sensitive radio telescopes. Finally, we note that the burst rate of FRB 20121102A in the CHIME band is the same as what is reported at 1.4 GHz (Cruces et al. 2020). This suggests that it is possible that FRB 20121102A has only been detected once in the CHIME band because of the comparatively low sensitivity of CHIME (Josephy et al. 2019), rather than solely due to either an intrinsically lower burst rate at ∼600 MHz (i.e., the source's luminosity peaks at higher frequencies) or propagation effects. Further monitoring of the FRB 20121102A source would aid in determining the most probable reason among the aforementioned potential explanations.

4. Summary and Conclusions

We present the host galaxies of four apparently nonrepeating FRBs, FRB 20181223C, FRB 20190418A, FRB 20191220A, and FRB 20190425A, that were first reported in CHIME/FRB Catalog-1. These FRBs are selected based on a planned hypothesis testing framework where only FRBs with low DM excess (<100 pc cm^{-3}), high Galactic latitude ($|b| > 10°$), and saved baseband data were considered. The baseband data facilitated the estimation of much more precise localization regions than the ones reported by CHIME/FRB Collaboration et al. (2021) using the CHIME/FRB baseband localization pipeline (Michilli et al. 2021). From our host follow-up studies, we identify only one host galaxy candidate in the deepest available archival images for each FRB. We then robustly associate the identified host candidates with their respective FRBs with chance association probabilities $<10\%$, after correcting for the look-elsewhere effect.

We also infer major host properties and SFHs of the host galaxies using `Prospector` with a nonparametric SFH model. Additionally, we search for possible multimessenger and multiwavelength counterparts, including GW events and compact persistent radio sources, within the 2σ baseband localization region of the FRBs and find none. Based on this null result, we derived a 3σ upper limit on the luminosity of compact radio sources at 3 GHz, effectively eliminating the possibility of a compact radio source similar to those observed in the cases of FRB 20121102A and FRB 20190520B. We note that the host of FRB 20190425A matches to what Moroianu et al. (2023) proposed based on the suggested association between GW190425 and FRB 20190425A. However, the association of GW190425 with UGC 10667 has already been shown to be unlikely by Bhardwaj et al. (2023), which renders the proposed GW–FRB association unlikely.

We also conduct an FRB host demographic analysis, considering only local Universe FRB hosts ($z < 0.1$) reported until 2023 July 31. Our choice of the maximum redshift limit is guided by the DM excess criterion within our planned hypothesis testing framework. This results in a sample of 18 local Universe FRB hosts, including the four reported in this study. We find all 18 FRB hosts to be spiral or late-type galaxies. The predominance of late-type galaxies suggests that the sources of FRBs are significantly younger than those of sGRBs and SNe Ia. More importantly, among all major FRB source formation channels proposed in the literature, CCSNe appear to be the dominant one. Moreover, our local Universe FRB host sample remains broadly consistent with the hosts of CCSNe. However, it is still possible that other formation channels contribute a limited number of sources to the overall FRB population. Furthermore, we compare the host properties

of repeating and apparently nonrepeating FRBs in our local Universe FRB sample. Our analysis does not reveal any significant evidence of discernible differences in their stellar populations.

Finally, considering their close proximity to Earth, we search the CHIME/FRB database for repeat bursts, between 2018 July 1 and 2021 May 1, from the four apparently nonrepeating FRBs and find none. Nonetheless, their burst rates fall within the range observed for localized CHIME/FRB repeating sources. Therefore, we encourage continued monitoring of these FRBs using more sensitive radio telescopes.

Acknowledgments

We thank the anonymous reviewer for their careful reading of our manuscript and their many insightful comments and suggestions. We thank the Dominion Radio Astrophysical Observatory, operated by the National Research Council Canada, for gracious hospitality and expertise. We acknowledge that CHIME is located on the traditional, ancestral, and unceded territory of the Syilx/Okanagan people. CHIME is funded by a grant from the Canada Foundation for Innovation (CFI) 2012 Leading Edge Fund (Project 31170) and by contributions from the provinces of British Columbia, Québec, and Ontario. The CHIME/FRB Project is funded by a grant from the CFI 2015 Innovation Fund (Project 33213), by contributions from the provinces of British Columbia and Québec, and by the Dunlap Institute for Astronomy and Astrophysics at the University of Toronto. Additional support was provided by the Canadian Institute for Advanced Research (CIFAR), McGill University and the McGill Space Institute via the Trottier Family Foundation, and the University of British Columbia. The Dunlap Institute is funded through an endowment established by the David Dunlap family and the University of Toronto. Research at Perimeter Institute is supported by the Government of Canada through Industry Canada and by the Province of Ontario through the Ministry of Research & Innovation. FRB research at UBC is supported by an NSERC Discovery Grant and by the Canadian Institute for Advanced Research. The CHIME/FRB baseband system is funded in part by a Canada Foundation for Innovation John R. Evans Leaders Fund award to I.H.S. The National Radio Astronomy Observatory is a facility of the National Science Foundation (NSF) operated under a cooperative agreement by Associated Universities, Inc. This work is based on data obtained as part of the Canada–France Imaging Survey, a CFHT large program of the National Research Council of Canada and the French Centre National de la Recherche Scientifique. Based on observations obtained with MegaPrime/MegaCam, a joint project of CFHT and CEA Saclay, at the Canada–France–Hawaii Telescope (CFHT), which is operated by the National Research Council (NRC) of Canada, the Institut National des Science de l'Univers (INSU) of the Centre National de la Recherche Scientifique (CNRS) of France, and the University of Hawaii. This work uses observations made with the Gran Telescopio Canarias (GTC), installed at the Spanish Observatorio del Roque de los Muchachos of the Instituto de Astrofísica de Canarias, in the island of La Palma. This research has made use of the NASA/IPAC Extragalactic Database (NED), which is operated by the Jet Propulsion Laboratory, California Institute of Technology, under contract with the National Aeronautics and Space Administration. This research has made use of the SIMBAD database and VizieR catalog access tool operated at CDS, Strasbourg, France.

M.B. is a McWilliams fellow and an International Astronomical Union Gruber fellow. M.B. also receives support from several McWilliams seed grants. V.M.K. holds the Lorne Trottier Chair in Astrophysics & Cosmology, a Distinguished James McGill Professorship, and receives support from an NSERC Discovery grant (RGPIN 228738-13), from an R. Howard Webster Foundation Fellowship from CIFAR, and from the FRQNT CRAQ. K.S. is supported by the NSF Graduate Research Fellowship Program. B.C.A. is supported by an FRQNT Doctoral Research Award. A.M.C. is funded by an NSERC Doctoral Postgraduate Scholarship. F.A.D. is supported by the UBC Four Year Fellowship. The Dunlap Institute is funded through an endowment established by the David Dunlap family and the University of Toronto. B.M.G. acknowledges the support of the Natural Sciences and Engineering Research Council of Canada (NSERC) through grant RGPIN-2022-03163 and of the Canada Research Chairs program. K.W.M. holds the Adam J. Burgasser Chair in Astrophysics and is supported by NSF grants (2008031, 2018490). C.L. is supported by NASA through the NASA Hubble Fellowship grant HST-HF2-51536.001-A awarded by the Space Telescope Science Institute, which is operated by the Association of Universities for Research in Astronomy, Inc., under NASA contract NAS5-26555. A.P. is funded by the NSERC Canada Graduate Scholarships—Doctoral program. A. B.P. is a Banting Fellow, a McGill Space Institute (MSI) Fellow, and a Fonds de Recherche du Quebec—Nature et Technologies (FRQNT) postdoctoral fellow. Z.P. is a Dunlap Fellow.

Facilities: CHIME, Gemini:Gillett, GTC, Magellan:Baade.

Software: Prospector (Leja et al. 2017; Johnson et al. 2019), FSPS (Conroy et al. 2009), MARZ (Hinton et al. 2016), dynesty (Speagle 2020), IRAF (Tody 1986, 1993), Fermi GBM data tools (Goldstein et al. 2021), Astropy (Astropy Collaboration et al. 2013, 2018), APLpy (Robitaille & Bressert 2012), SAOImage DS9 (Joye & Mandel 2003), NumPy (Harris et al. 2020), Matplotlib (Hunter 2007).

Appendix A
Stellar Population Synthesis Using `Prospector`

To determine the properties of the stellar population in the FRB host galaxies, we employ a Python-based Bayesian inference code, `Prospector` (Leja et al. 2017; Johnson et al. 2019). It generates model SEDs using stellar population synthesis models defined within the framework of the Flexible Stellar Populations Synthesis stellar populations code (Conroy et al. 2009). By fitting the archival photometry data with `Prospector` using a nested sampling fitting routine called `dynesty` (Speagle 2020), we obtain posterior distributions for the stellar population properties of interest, which include the age of the galaxy at the time of observation (with the maximum allowed value being the age of the universe at the redshift of the FRB host), total mass formed, stellar metallicity ($\log(Z/Z_{\odot})$), and V-band optical depth.

In all our fits using `Prospector`, we adopt the Chabrier (2003) initial mass function (IMF) and utilize a nonparametric continuity_flex_sfh with nine SFH bins (Leja et al. 2019a). In this model, the edges of the time bins are adjusted so that for a given set of SFRs the same amount of mass forms in each bin. The SFRs from both old and young populations in each time

Table 5
Free Parameters and Their Associated Priors for the `Prospector` "Continuity_flex_sfh" Model

Parameter	Description	Prior
$\log(M/M_{\odot})$	total stellar mass formed	uniform: min = 8, max = 12.0
$\log(Z_{*}/Z_{\odot})$	stellar metallicity	clipped normal: min = −0.5, max = 1.0, mean and σ following Leja et al. (2019b) mass–metallicity prior
$\hat{\tau}_{\lambda,2}$	diffuse dust optical depth	uniform: min = 0.0 mag, max = 2.5 mag
n	slope of Kriek & Conroy (2013) dust attenuation curve	uniform: min = −1.0, max = 4.0
$f_{\rm AGN}$	fraction of total AGN luminosity relative to the bolometric stellar luminosity	log uniform: min = 10^{-5}, max = 3
$\tau_{\rm AGN}$	optical depth of the AGN dust torus	log uniform; min = 5, max = 150
$\log(\rm SFR_{ratio,young})$	ratio of SFR in youngest bin to last flex bin	Student's t (mean = 0, scale = 0.3, df = 2)
$\log(\rm SFR_{ratio,old})$	3-vector array; ratio of SFR in old bins to first flex bin	Student's t (mean = 0, scale = 0.3, df = 2)
$\log(\rm SFR_{ratio})$	4-vector array; ratio of SFR in flex bins	Student's t (mean = 0, scale = 0.3, df = 2)

Table 6
Twelve Broadband Filters Used to Model the SED of FRB 20181220A

Instrument[a]	Filter	Effective Wavelength (Å)	Flux Density[b,c] (maggies)
SWIFT/UVOT[b]	w1	2600	2.80×10^{-8}
Pan-STARRS DR2[d]	*g*	3546	5.95×10^{-7}
	r	4670	8.67×10^{-7}
	i	6156	1.08×10^{-6}
	z	7472	1.29×10^{-6}
	y	8917	1.60×10^{-6}
2MASS	*J*	12319	2.28×10^{-6}
	H	16420	2.82×10^{-6}
	Ks	21567	2.38×10^{-6}
WISE	W1	33461	1.11×10^{-6}
	W2	45952	6.84×10^{-7}
	W3	115526	4.00×10^{-6}

Notes.
[a] For all instruments' flux densities, the aperture used for estimating respective magnitudes is larger than twice the effective size of the galaxies.
[b] Note that 1 maggie is defined as the flux density in janskys divided by 3631. Fluxes at $\lambda < 100000$ Å are corrected for Galactic extinction according to the prescription of Schlafly & Finkbeiner (2011).
[c] All broadband fluxes are assigned a 20% fractional uncertainty.
[d] The SWIFT/UVOT w1 flux density is extinction and inclination angle corrected, taken from the Swift/UVOT Serendipitous Source Catalog (Yershov 2014).

Table 7
Thirteen Broadband Filters Used to Model the SED of the FRB 20181223C Host

Instrument[a]	Filter	Effective Wavelength (Å)	Flux Density[b,c] (maggies)
GALEX[b]	FUV	1549	2.29×10^{-8}
	NUV	2304	3.77×10^{-8}
SDSS[c]	*u*	3546	4.44×10^{-8}
	g	4670	1.30×10^{-7}
	r	6156	2.01×10^{-7}
	i	7472	2.48×10^{-7}
	z	8917	2.26×10^{-7}
UKIRT[a]	J	12480	2.70×10^{-7}
	H	16310	2.92×10^{-7}
	K	22010	2.04×10^{-7}
WISE[c]	W1	33461	1.44×10^{-7}
	W2	45952	8.44×10^{-8}
	W3	115526	2.69×10^{-7}

Notes.
[a] From United Kingdom Infrared Telescope (UKIRT) Infrared Deep Sky Survey (UKIDSS) Data Release 9 (Lawrence et al. 2013), where Kron magnitudes are estimated using the same aperture size employed by Chang et al. (2015).
[b] From the SPRING catalog (Cattorini et al. 2023).
[c] SDSS and WISE filters' flux densities are obtained from the aperture-matched photometry catalog of nearby galaxies by Chang et al. (2015).

bin are determined using the "continuity" prior, which places a Student's t prior on the log of the ratio of the SFR in adjacent bins ("log $\rm SFR_{ratio}$"). This prior encourages smooth SFHs, where the SFR does not jump significantly between each time bin. However, sharp burst or quenching events are still allowed. Note that the edges of the first and last time bins are fixed, which are ≈10 Gyr (to cover the first 1.5 Gyr of the galaxy's history) and 10 Myr (to capture the most recent SFR) look-back time, respectively, in our runs. However, the edges of the other seven time bins are allowed to vary. These bins are used to capture the SFR at certain epochs in the SFH such that each bin forms an equal stellar mass. Note that this allows for more flexibility in the duration, start time, and end time of the recent burst: the SFR can change at an arbitrary time, as opposed to only changing at the edges of fixed time bins. In our case, we use default Student's t prior values of its three parameters, which are described in Table 5.

We also fix the model redshifts to the spectroscopic redshifts of the FRB host galaxies and add nebular emission (Byler et al. 2017) to the SED using the default fixed parameters in `Prospector`. To ensure realistic masses corresponding to a given stellar metallicity, we constrain the total mass formed and stellar metallicities using the Gallazzi et al. (2005) mass–metallicity relation. For measuring dust attenuation, we employ the Kriek & Conroy (2013) model, which includes a sampled parameter determining the offset from the Calzetti et al. (2000) attenuation curve. Furthermore, following Wild et al. (2020), we fix the birth-cloud optical depth to the same value as the diffuse optical depth. This implies that young stars are attenuated twice as much as old stars. We also set the dust emission parameters such that the warm dust fraction is fixed to 0.01, the minimum radiation field is fixed to 1.0, and the polycyclic aromatic hydrocarbon mass fraction is fixed to 2%, as proposed by Leja et al. (2019a). Furthermore, because all four FRB host galaxies have available 2MASS and WISE data,

Table 8
Eleven Broadband Filters Used to Model the SED of FRB 20190418A

Instrument	Filter	Effective Wavelength (Å)	Flux Density (maggies)
SDSS	*u*	3546	6.83×10^{-8}
	g	4670	1.88×10^{-7}
	r	6156	2.78×10^{-7}
	i	7472	3.51×10^{-7}
	z	8917	3.98×10^{-7}
2MASS	*J*	12319	4.14×10^{-7}
	H	16420	3.83×10^{-7}
UKIRT	WFCAM *K*	22010	3.03×10^{-7}
WISE	W1	33461	1.87×10^{-7}
	W2	45952	1.12×10^{-7}
	W3	115526	4.59×10^{-7}

Table 9
Fourteen Broadband Filters Used to Model the SED of FRB 20190425A

Instrument	Filter	Effective Wavelength (Å)	Flux Density[a,b] (maggies)
GALEX[a]	FUV	1549	4.41×10^{-8}
	NUV	2304	7.70×10^{-8}
SDSS[b]	*u*	3546	2.08×10^{-7}
	g	4670	6.31×10^{-7}
	r	6156	1.07×10^{-6}
	i	7472	1.43×10^{-6}
	z	8917	1.87×10^{-6}
2MASS[c]	J	12319	2.46×10^{-6}
	H	16420	2.71×10^{-6}
	Ks	21567	1.92×10^{-6}
WISE[b]	W1	33461	1.55×10^{-6}
	W2	45952	9.37×10^{-7}
	W3	115526	6.49×10^{-6}
	W4	220783	4.65×10^{-6}

Notes.
[a] GALEX-calibrated and extinction-corrected fluxes are taken from Bianchi et al. (2017).
[b] SDSS and WISE filters' flux densities are obtained from the aperture-matched photometry catalog of nearby galaxies by Chang et al. (2015).
[c] For 2MASS filter magnitudes, we used Kron magnitudes from Skrutskie et al. (2006) with the same aperture size used by Chang et al. (2015), thus ensuring accurate and comparable measurements.

we incorporate the Draine & Li (2007) infrared dust emission model, which consists of three components.

Given that all four FRB host galaxies have WISE magnitudes available, we also included the AGN dust torus emission described by two parameters, $f_{\rm AGN}$ and $\tau_{\rm AGN}$ (Nenkova et al. 2008; Leja et al. 2018), to account for a possible AGN contribution to the mid-IR part of the SED. It is worth noting that our fitting process does not indicate evidence of a significant AGN contribution in our FRB hosts' SED ($f_{\rm AGN} < 1\%$). This is also evident from the WISE color–color diagnostics discussed in Section 3.1.1.

Finally, to calculate the stellar mass, present-day SFR, and mass-weighted age for each host, we follow the methods outlined in Bhardwaj et al. (2021b).

Tables 6–9 list the different broadband filter fluxes used in our SED fitting for the host galaxies of FRB 20181220A, FRB 20181223C, FRB 20190418A, and FRB 20190425A, respectively, which are shown in Figures 9 and 10. Note that all flux densities are estimated after correcting for Milky Way extinction. All derived host galaxy properties from this analysis are provided in Table 2. The quoted uncertainties in all cases are 1σ values.

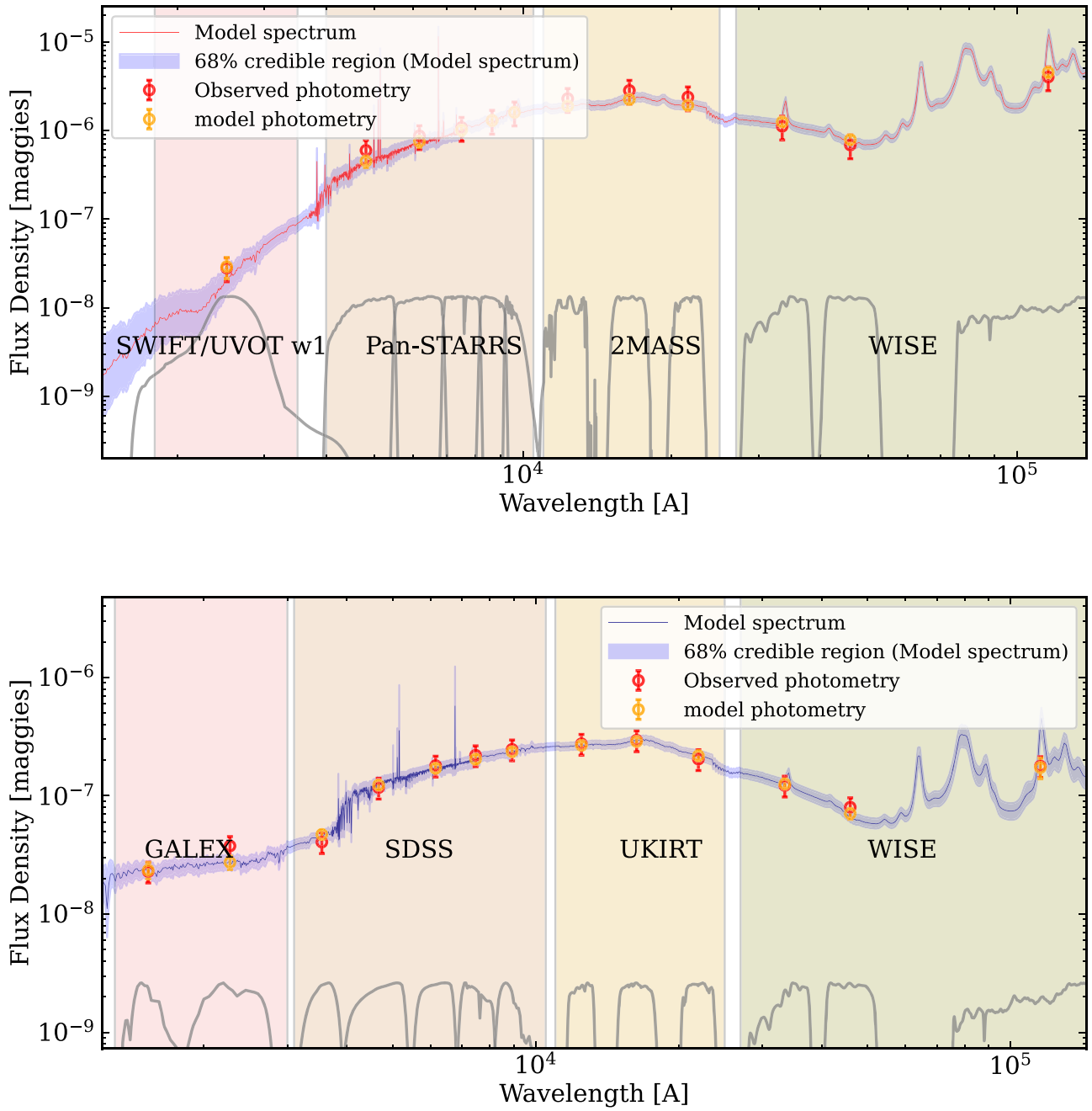

Figure 9. The best-fitted SED model of the host galaxies of FRB 20181220A (top) and FRB 20181223C (bottom). The flux densities of the host galaxies in different wavelength bands are plotted along with the best-fit `Prospector` model spectrum. To assess the quality of the `Prospector` models, the modeled and actual photometry data are also shown. For more information, see Appendix A.

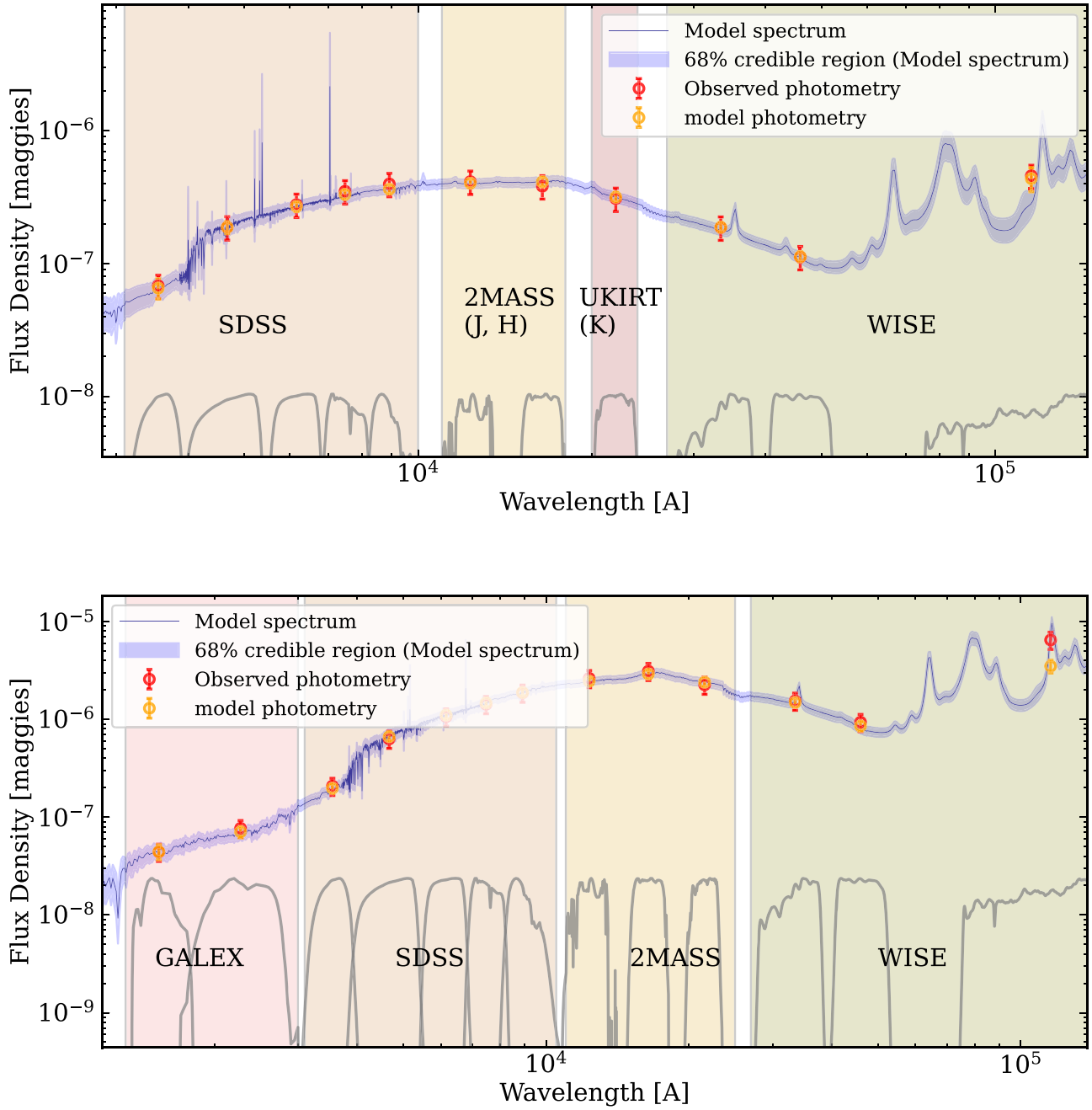

Figure 10. Same as Figure 9, but for the best-fitted SED model of the host galaxies of FRB 20190418A (top) and FRB 20190425A (bottom).

Appendix B
Spectroscopic Observations of FRB 20181223C

We obtained the spectroscopic redshift of four host galaxy candidates in the FRB 20181223C 2σ localization region (Sources 1, 2, 3, and 4 in Figure 3) using observations performed with the Optical System for Imaging and low-Intermediate-Resolution Integrated Spectroscopy (OSIRIS) instrument at the GTC on 2021 February 18.[32] To optimize the observations, we separated the targets in two observing blocks (OBs) to use both the long-slit and the multiobject spectroscopy (MOS) capabilities of OSIRIS.

For the MOS OB, we designed a mask with the OSIRIS Mask Designer Tool (González-Serrano et al. 2004; Gómez-Velarde et al. 2016), using four fiducial stars and catalog coordinates of the host galaxy candidates. The mask contained rectangular slitlets with lengths between 10″ and 20″.

The observations were performed during dark/gray time under clear conditions, with seeing of ∼1″ and air mass between 1.05 and 1.3. Three 1200 s and two 1000 s exposures were taken in the respective MOS and long-slit configurations. We used the R500B grism covering the spectral range 3600 −7200 Å. The slit width was 1.″5 in both observing modes. The spectral resolution was ∼21 Å.

The spectra from both OBs were reduced using the GTCMOS pipeline (Gómez-González et al. 2016), which uses IRAF routines (Tody 1986, 1993). To calibrate the flux, we used the spectrophotometric standard G191-B2B (Oke 1974, 1990; Massey et al. 1988) observed during the same night as the target galaxies. For the

[32] Program GTCMULTIPLE3B-20BMEX.

Table 10
Galaxies from the PS1−STRM Catalog in the 2σ Localization Region of FRB 20181223C

#	R.A. (J2000)	Decl. (J2000)	Krmag	Redshift
1	$12^h03^m40\overset{s}{.}98$	$27°39'51\overset{''}{.}4$	16.97	0.03024(1)
2[a]	$12^h03^m40\overset{s}{.}04$	$27°32'44\overset{''}{.}5$	19.89	0.23932(2)
3	$12^h03^m44\overset{s}{.}53$	$27°32'55\overset{''}{.}9$	20.43	0.274(1)
4	$12^h03^m46\overset{s}{.}72$	$27°32'46\overset{''}{.}9$	20.71	0.371(1)

Notes. Redshifts have been measured using the GTC telescope. Galaxy PSO J120340.98+273251.4, aka Source 1, is the most probable host in the field given its low redshift. The spectroscopic redshift of Source 2 is estimated using the Magellan telescope.
[a] The spectroscopic redshift of Source 2 is estimated using 1D spectra obtained using the 6.5 m Magellan Baade Telescope at LCO.

wavelength calibration we used arc-lamp spectra of Ne, Hg, and Ar. The rms errors of the resulting solutions were <2 Å.

We extracted the calibrated spectra from the resulting 2D product, identified lines for each of the five observed galaxies, and estimated their redshifts. The results were verified by comparing the extracted spectra with the galaxy templates from the Manual and Automatic Redshifting Software (MARZ; Hinton et al. 2016).

For Source 2, we took spectroscopic observation using the IMACS wide-field imaging spectrograph on the 6.5 m Magellan Baade Telescope at Las Campanas Observatory (LCO). The observations were taken on 2022 February 21, with an observing air mass from 1.8 to 2.0 and seeing at approximately $0\overset{''}{.}8$. We took five 300 s exposures using a $0\overset{''}{.}9$-long slit mask and a 150 line mm^{-1} grism. Using IRAF, the frames were corrected using bias and flats frames. Arc-lamp exposures from He, Ne, and Ar were used in order to obtain a wavelength calibration spectrum, which was then used to reshape the corrected science frames. Finally, the spectroscopic redshift of Source 2 was estimated to be $z_{\rm spec} = 0.23932 \pm 0.00002$ using Hα, Hβ, [O III], and [S II] emission lines.

The corresponding redshifts are presented in Table 10.

Appendix C
Local Universe FRB Host Sample

In this appendix, we delve into major observational evidence pertaining to the morphology and structural characteristics of the galaxies in our sample of robustly associated local Universe FRB hosts as discussed in Section 3.1, which lends support to their classification as spiral galaxies. As detailed in Section 3.1, the presence of discernible spiral arms serves as the most compelling evidence for identifying a host galaxy as a spiral. However, in situations where the resolution or sensitivity of archival optical images is insufficient to reveal the distinctive spiral arm features, alternative structural attributes, such as the presence of a well-defined disk coupled with ongoing star formation, prove invaluable in distinguishing late-type spirals from early-type disk galaxies, notably lenticular galaxies (Blanton & Moustakas 2009; Vika et al. 2015).

Lenticular galaxies have a structure that appears intermediate between elliptical galaxies (characterized by a dominant bulge component) and spiral galaxies (distinguished by their disk morphology but lacking spiral arms; van den Bergh 1979). Their structural resemblance to elliptical galaxies is further accentuated by the fact that they have used up or lost most of their interstellar matter and therefore have very little ongoing star formation (van den Bergh 2009). This unique characteristic aligns them with elliptical galaxies. In instances where a clear disk is noted with a weak or nonexistent bulge and the host shows ongoing star formation, we consider the galaxy as a late-type spiral instead of a lenticular galaxy, as suggested by Kennicutt (1998) and Brennan et al. (2015).

We now discuss major morphological features of each FRB host galaxy in our sample.

FRB 20200120E: FRB 20200120E is the closest extragalactic repeating FRB detected by the CHIME/FRB project (Bhardwaj et al. 2021a), which is localized to a GC of M81 (Kirsten et al. 2022), a nearby grand-design spiral galaxy at 3.6 Mpc (Buta 2019) with with $P_{\rm cc} < 0.1\%$ (Kirsten et al. 2022). Figure 11 shows the Digital Sky Survey r-band image of M81.

FRB 20181030A: FRB 20181030A is the second-closest extragalactic repeating FRB first reported by CHIME/FRB Collaboration et al. (2019). Subsequently, using CHIME/FRB baseband localization of the FRB, Bhardwaj et al. (2021b) reported the host galaxy of the FRB to be NGC 3252, an Sd-type spiral galaxy at 20 Mpc (Mager et al. 2018; Hong et al. 2019), with $P_{\rm cc} < 1\%$. The Pan-STARRS r-band image of NGC 3252 is presented in Figure 11.

FRB 20171020A: FRB 20171020A is a low-DM apparently nonrepeating FRB (DM = 114 pc cm^{-3}) discovered by ASKAP. Mahony et al. (2018) identified the likely host of the FRB to be ESO 601-36, an Sc-type spiral galaxy (Lauberts 1982) at a redshift of $z = 0.00867$ (Meyer et al. 2004), with a $P(O|x) \approx 98\%$ (Lee-Waddell et al. 2023). The Pan-STARRS r-band image of ESO 601-36 is shown in Figure 11.

FRB 20220319D: FRB 20220319D is an apparently nonrepeating FRB discovered and localized by the DSA-110 to a barred spiral galaxy IRAS 02044+7048 (Hau et al. 1995), at 50 Mpc (Ravi et al. 2023b) with a chance association probability $\leqslant 10^{-4}$. In Figure 11, we showed the SDSS r-band image of the host galaxy.

FRB 20181220A: Discussed in Section 2.2.1. The Pan-STARRS r-band image of the host galaxy, 2MFGC 17440, is displayed in Figure 11.

FRB 20181223C: Discussed in Section 2.2.2. The DESI r-band image of the host galaxy, SDSS J120340.98+273251.4, is shown in Figure 11.

FRB 20190425A: Discussed in Section 2.2.4. The DESI r-band image of UGC 10667, the host galaxy of FRB 20190425A, is shown in Figure 11.

FRB 20180916B: FRB 20180916B is a repeating FRB discovered by CHIME/FRB Collaboration et al. (2019), which was later localized to the nearby massive nearly face-on spiral galaxy SDSS J015800.28+654253.0 (see Figure 11; from Tendulkar et al. 2021) at redshift $z = 0.0337$ (Marcote et al. 2020), with $P_{\rm cc} \leqslant 0.1\%$.

FRB 20220207C: FRB 20220207C is an apparently nonrepeating FRB localized by the DSA-110 to a nearby galaxy, PSO J310.1977+72.8826 (Law et al. 2024). From the Pan-STARRS r-band optical image of the host shown in Figure 11, it is a nearly edge-on disk-dominated galaxy with the index of the best-fitted Sérsic profile ≈ 0.5. Using the formalism discussed by Pannella et al. (2006), the galaxy is likely to have the Hubble T-type morphological classification >2, suggesting that the host is a late-type spiral galaxy. Finally, Law et al. (2024) noted that the host has a high SFR (2.1 $M_\odot$ yr^{-1}), which, along with its disk-dominated morphology, supports it being a late-type spiral galaxy.

FRB 20211127I: FRB 20211127I is an apparently nonrepeating FRB localized by ASKAP (Gordon et al. 2023) to a

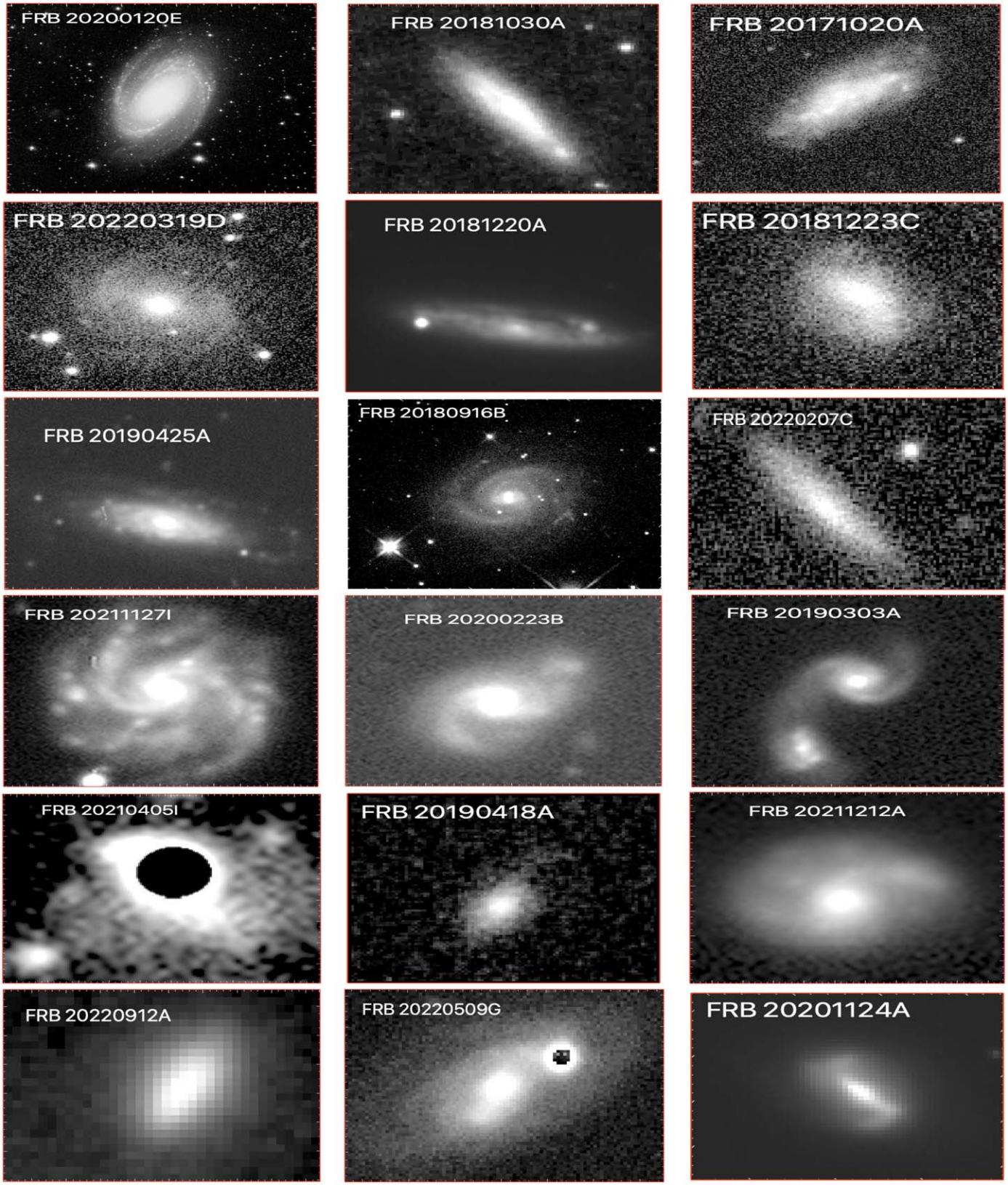

Figure 11. Host galaxies of 18 local Universe FRBs used in this study, with black circles masking stars overlapping FRB 20210405I and FRB 20220509G hosts. For additional information, see Appendix C.

nearby grand-design spiral galaxy, 6dFGS J131914.0–185017, at $z = 0.04695$, with a $P(O|x) > 99\%$ (Glowacki et al. 2023). The DESI r-band image of the host is shown in Figure 11.

FRB 20200223B: FRB 20200223B is a repeating FRB reported by CHIME/FRB Collaboration et al. (2023). Using the CHIME/FRB baseband localization, Ibik et al. (2024)

identified LEDA 1847306 or SDSS J003304.68+284952.6 (the SDSS *r*-band image is shown in Figure 11), an Scd-type spiral galaxy (Kuminski & Shamir 2016), as its most likely host at $z = 0.060235$, with a $P(O|x) > 90\%$.

FRB 20190303A: FRB 20190303A is a repeating FRB detected by the CHIME/FRB project (Fonseca et al. 2020). Using the subarcminute localization precision, Michilli et al. (2023) associated the FRB with a pair of merging spiral galaxies (the SDSS *r*-band image of the merger system is shown in Figure 11), SDSS J135159.17+480729.0 and J135159.87+480714.2 (Vorontsov-Vel'Yaminov & Arkhipova 1962), located at a redshift of $z = 0.064$ (Ahn et al. 2012), with a $P(O|x) > 99\%$.

FRB 20210405I: FRB 20210405I is an apparently nonrepeating FRB detected using MeerKAT (Driessen et al. 2024) and was also observed commensally with the ThunderKAT survey (Fender et al. 2016), which facilitated its subarcsecond localization and subsequent association with a nearby galaxy named 2MASS J1701249–4932475 at a redshift of $z = 0.066$, with $P_{cc} < 1\%$. Driessen et al. (2024) identify the morphology of the galaxy to be a spiral in the DECaPS2 DR2 *r*-band image (Saydjari et al. 2023) as shown in Figure 11. Moreover, the high inferred SFR of the host as inferred by Driessen et al. (2024) is consistent with it being a star-forming spiral galaxy.

FRB 20190418A: Discussed in Section 2.2.3. The UKIDSS-DR9 GCS *K*-band image of the host is shown in Figure 11.

FRB 20211212A: FRB 20211212A is an apparently nonrepeating FRB discovered by ASKAP (Gordon et al. 2023). Using the subarcsecond localization of the FRB, Gordon et al. (2023) localized it to a star-forming spiral galaxy, SDSS J102924.22+012139.2, at $z = 0.0707$ (Kuminski & Shamir 2016), as can be inferred from the *r*-band DESI image of the host shown in Figure 11.

FRB 20220912A: FRB 20220912A is a highly active repeating FRB that was discovered by the CHIME/FRB project (McKinven & CHIME/FRB Collaboration 2022). The FRB was localized to a disk-dominated galaxy with a moderate SFR ($\approx 0.1\, M_{\odot}\, \mathrm{yr}^{-1}$) at $z = 0.077$ by Ravi et al. (2023a). This is supported by the fact that the best-fitted Sérsic profile has an index = 1, suggesting that it is a disk galaxy with a low degree of central concentration (bulge-to-total luminosity ratio $\leqslant 0.2$; Mancini et al. 2015; Davari et al. 2016). This suggests that the FRB host likely has a Hubble sequence classification >0 (Baillard et al. 2011), which makes it likely a late-type spiral galaxy. The GTC *r*-band image of the host galaxy is shown in Figure 11.

FRB 20220509G: Discussed in Appendix D. The CFIS DR3 *r*-band image of the FRB 20220509G host is shown in Figure 11.

FRB 20201124A: FRB 20201124A is a repeating FRB first detected by the CHIME/FRB project (Lanman et al. 2022). It was localized to a galaxy named SDSS J050803.48+260338.0 at $z = 0.098$ by ASKAP (Fong et al. 2021), the Very Large Array (Ravi et al. 2022), and the European Very Long Baseline Interferometry Network (Nimmo et al. 2022), with $P_{cc} \leqslant 0.1\%$. Xu et al. (2022), using the 10 m Keck telescopes, identified SDSS J050803.48+260338.0 as a barred spiral galaxy (shown in Figure 11).

Appendix D
Nature of the Host of FRB 20220509G

Sharma et al. (2023) and Connor et al. (2023) claimed that the FRB 20220509G host is a quiescent, elliptical (hence early-type) galaxy. This would make it the only FRB localized to an elliptical galaxy, as well as an outlier among all the local Universe FRBs considered in Section 3.1.1. However, the FRB host is classified as a spiral based on the WISE color–color classification discussed in Section 3.1.1. Moreover, there is an indication of a barlike extended structure in the host galaxy Pan-STARRS image presented by Sharma et al. (2023). However, the tentative detection of a "barlike" structure is not strong enough to claim that it is a spiral galaxy. Therefore, we searched for a deeper image in different optical archival surveys and found a deeper *r*-band image of the FRB FOV in the CFIS legacy survey data release 3 (Ibata et al. 2017; Fantin et al. 2019), with a median point-source depth of $5\sigma = 25$ AB mag.[33]

The FRB 20220509G host galaxy detected in the CFIS DR3 *r*-band image is shown in Figure 5, where we clearly see the host's extended spiral arm and barlike morphological features. Hence, we classify the FRB host as a spiral, and hence a late-type galaxy, in Section 3.1.1.

Appendix E
Pantheon Sample of Type Ia Supernovae

The Pantheon cosmological SN sample (Scolnic et al. 2018) is the largest spectroscopic sample of SNe Ia available, comprising a total of 1047 SNe Ia with redshifts spanning from $0.01 < z < 2.3$. For a subset of 330 SNe Ia from the Pantheon sample, Pruzhinskaya et al. (2020) reported their host morphology. They classified visually the 330 galaxies into the following five morphological classes: spheroid (E/S0), spheroid+disk (S0/Sa), disk (Sb/Sbc/Sc), disk+irregular (Sc/Scd), and irregular (Scd/Ir). Furthermore, Pruzhinskaya et al. (2020) categorize galaxies with morphological classes "E," "E/S0," "Pa," and "S0" as early-type galaxies and those with classes "S0/a," "Sa," "Sab," "Sb," "Sbc," "Sc," "Scd," "Sd," "SF," and "Ir" as late-type galaxies. For our analysis, we consider a subset of those SN Ia host galaxies with $z \leqslant 0.1$, which gives us a sample of 193 SN Ia host galaxies, consisting of 46 early-type galaxies and 147 late-type galaxies. Figure 12 shows the distribution of 193 SN Ia host galaxies in each of the aforementioned morphological categories. Based on this, we

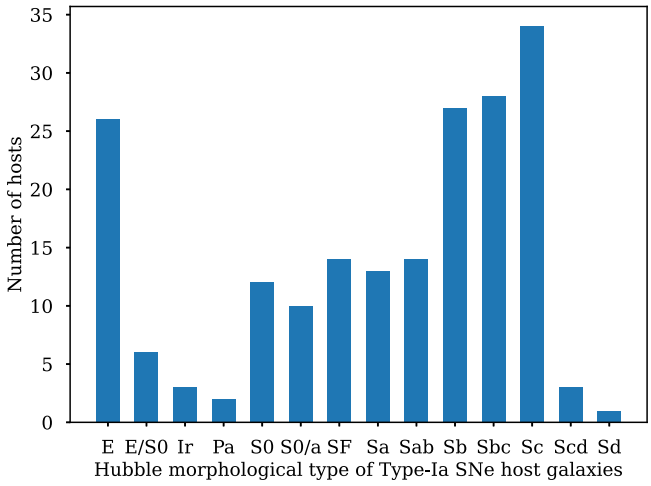

Figure 12. Distribution of the host galaxies of the Pantheon SN Ia subsample according to their morphological classes as discussed in Appendix E. For more details on the classification scheme, see Pruzhinskaya et al. (2020).

[33] The FRB FOV image is accessed via the Canadian Astronomy Data Centre: https://www.cadc-ccda.hia-iha.nrc-cnrc.gc.ca/en/search/.

estimate the fraction of "late-type" galaxies in the sample to be 0.76. This fraction serves as the null hypothesis against which we conduct a comparison with the local Universe FRB host sample, as elaborated in Section 3.1.2.

Appendix F
Local Universe FRBs' Star Formation Rates and Stellar Masses: Implications for the Progenitors

In Section 3.1.2, we argued, based on the preponderance of local Universe spiral hosts, that CCSNe are likely the dominant channel to form FRB sources. In this appendix, we examine the similarities between the local Universe FRB host sample and CCSN hosts based on their host galaxies' physical properties, such as SFR and stellar mass. Furthermore, among various CCSN channels, we focus here on SN II CCSNe because of their relatively large volumetric rate ($\sim 10^5\,\mathrm{Gpc^{-3}\,yr^{-1}}$;[34] Bazin et al. 2009) and possible connection with Galactic magnetar SGR 1935+2154 (see Section 1). Moreover, no significant statistical differences among the host galaxies of SNe Ib, SNe Ic, and SNe II have been noted in the literature (Anderson et al. 2012; Eldridge et al. 2013; Galbany et al. 2014).

To compare our local Universe FRB host sample with that of SN II hosts, we use the Palomar Transient Factory Core-collapse Supernova Host-galaxy catalog (Schulze et al. 2021).[35] We consider those SNe II (1) discovered at $z < 0.1$ and (2) for which independent and consistent spectroscopic redshift measurements for both the SNe II and their associated host galaxies are available. To check for the host galaxy redshift, we use the SDSS Data Release 16 (DR16) catalog (Ahumada et al. 2020). This yields a sample of 83 SN II host galaxies, which forms the basis of our comparative analyses discussed below.

From the SFR versus stellar mass plot shown in Figure 13, it can be noted that most SN II host galaxies (≈83%) are located above the star-forming MS (SFMS) region threshold (the dotted blue line that separates star-forming and green valley regions in Figure 13). This is expected, as SNe II mark the endpoints in the lives of short-lived (lifetime $\lesssim$few $\times\, 10^7$ yr) but massive stars ($M \gtrsim 8\,M_\odot$), making their detection more probable within galaxies undergoing active star formation. In comparison, we note the lower fraction of local Universe FRB host galaxies located in the star-forming region (≈67%). However, using the binomial statistics discussed in Sections 3.1.1 and 3.1.2, the relatively lower presence of FRB hosts in the SFMS region, in contrast to SN II hosts, lacks statistical significance ($p > 0.07$) and can be attributed to the modest sample size and unaccounted-for selection effects within our local Universe FRB host sample (see Section 3.1). Similar insights emerge from the color−absolute magnitude plot shown in Figure 13. Notably, local Universe FRBs exhibit a discernible yet statistically modest surplus in the fraction of red-sequence galaxies (50%) compared to SN II hosts (37%) using the color–magnitude threshold defined by Bernardi et al. (2010) to select red-sequence galaxies (above the dotted blue line in Figure 13). Therefore, we find the host galaxies of local Universe FRBs to be consistent with those of Type II CCSNe.

[34] This aligns well with the high occurrence of FRBs, $\sim 10^5$ FRBs $\mathrm{yr^{-1}}$ $\mathrm{Gpc^{-3}}$ at a fiducial energy of $\sim 10^{39}$ erg (Shin et al. 2023).
[35] The catalog can be accessed from here: 10.26093/cds/vizier.22550029.

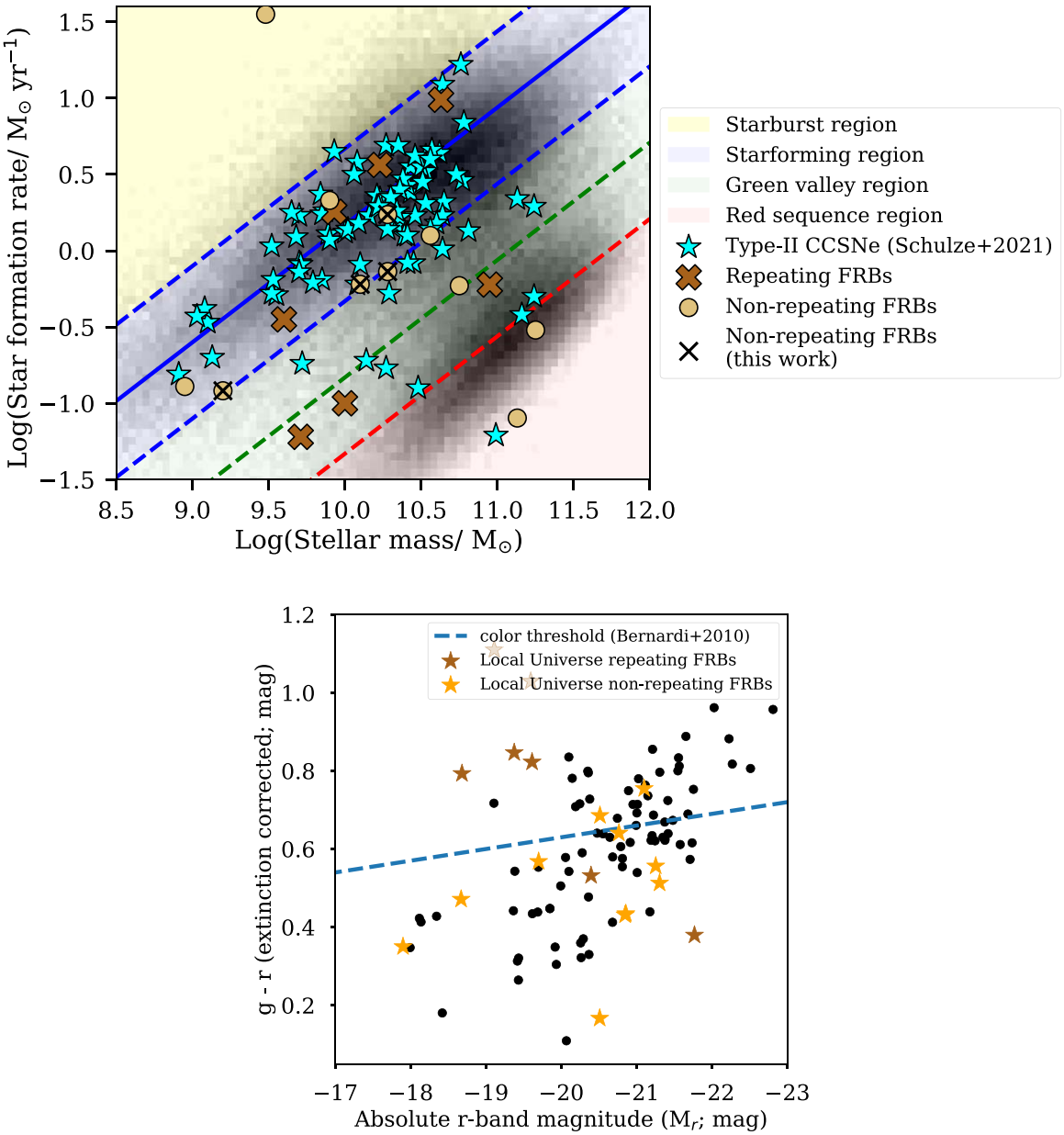

Figure 13. Comparison of notable physical properties of the host galaxies of 18 local Universe FRBs and 83 SNe II. The sample of host galaxies of SNe II (represented as cyan stars) is taken from the Palomar Transient Factory (PTF) Core-collapse Supernova Host-galaxy catalog (Schulze et al. 2021). Our local Universe FRB sample consists of 7 repeating FRBs (bold crosses) and 11 apparently nonrepeating FRBs (circles). The four apparently nonrepeating FRBs presented in this work can be differentiated from other apparently nonrepeating FRBs via the crosses overlaid. Top: SFR vs. total stellar mass (M_*) for local Universe FRBs and PTF SN II hosts. The background population of galaxies is taken from the SDSS MPA-JHU DR7 catalog (Brinchmann et al. 2004). The solid blue line represents the SFMS (Peng et al. 2010). Following the framework developed by Law-Smith et al. (2017), dashed lines are spaced $1\sigma = 0.5$ dex apart (the median scatter in SFMS), with the green valley falling 1σ–3σ below the SFMS (the region between the lower blue dashed line and red dashed line). The galaxies below the red dashed line are found to be quiescent. These lines are used to define four regions that are shaded and labeled in the figure. Bottom: rest-frame color–magnitude diagram of the host galaxies of FRBs (stars) compared to those of Type II CCSNe (black circles). The rest-frame colors and absolute r-band magnitude of FRBs are taken from their discovery papers, or in cases where those values are missing, we estimate them using the host photometry magnitudes in the Pan-STARRS release 1 (PS1) survey catalog data (Chambers et al. 2016).

ORCID iDs

Mohit Bhardwaj https://orcid.org/0000-0002-3615-3514
Daniele Michilli https://orcid.org/0000-0002-2551-7554
Aida Yu. Kirichenko https://orcid.org/0000-0002-8139-8414
Obinna Modilim https://orcid.org/0009-0005-0466-9371
Kaitlyn Shin https://orcid.org/0000-0002-6823-2073
Victoria M. Kaspi https://orcid.org/0000-0001-9345-0307
Bridget C. Andersen https://orcid.org/0000-0001-5908-3152
Tomas Cassanelli https://orcid.org/0000-0003-2047-5276
Charanjot Brar https://orcid.org/0000-0002-1800-8233
Shami Chatterjee https://orcid.org/0000-0002-2878-1502
Amanda M. Cook https://orcid.org/0000-0001-6422-8125
Fengqiu Adam Dong https://orcid.org/0000-0003-4098-5222
Emmanuel Fonseca https://orcid.org/0000-0001-8384-5049
B. M. Gaensler https://orcid.org/0000-0002-3382-9558
Adaeze L. Ibik https://orcid.org/0000-0003-2405-2967
J. F. Kaczmarek https://orcid.org/0000-0003-4810-7803

Adam E. Lanman https://orcid.org/0000-0003-2116-3573
Calvin Leung https://orcid.org/0000-0002-4209-7408
K. W. Masui https://orcid.org/0000-0002-4279-6946
Ayush Pandhi https://orcid.org/0000-0002-8897-1973
Aaron B. Pearlman https://orcid.org/0000-0002-8912-0732
Emily Petroff https://orcid.org/0000-0002-9822-8008
Ziggy Pleunis https://orcid.org/0000-0002-4795-697X
J. Xavier Prochaska https://orcid.org/0000-0002-7738-6875
Masoud Rafiei-Ravandi https://orcid.org/0000-0001-7694-6650
Ketan R. Sand https://orcid.org/0000-0003-3154-3676
Paul Scholz https://orcid.org/0000-0002-7374-7119
Kendrick M. Smith https://orcid.org/0000-0002-2088-3125

References

Abbott, B. P., Abbott, R., Abbott, T. D., et al. 2020, ApJL, 892, L3
Abdurro'uf, Accetta, K., Aerts, C., et al. 2022, ApJS, 259, 35
Aggarwal, K., Budavári, T., Deller, A. T., et al. 2021, ApJ, 911, 95
Ahn, C. P., Alexandroff, R., Allende Prieto, C., et al. 2012, ApJS, 203, 21
Ahumada, R., Allende Prieto, C., Almeida, A., et al. 2020, ApJS, 249, 3
Anderson, J. P., Habergham, S. M., James, P. A., & Hamuy, M. 2012, MNRAS, 424, 1372
Anderson, L. D. 2001, Empirical Direction in Design and Analysis, Scientific Psychology Series (London: Taylor and Francis), https://books.google.com/books?id=3Fh6AgAAQBAJ
Anderson, L. D., Bania, T., Balser, D. S., et al. 2014, ApJS, 212, 1
Astropy Collaboration, Price-Whelan, A. M., Sipőcz, B. M. ., et al. 2018, AJ, 156, 123
Astropy Collaboration, Robitaille, T. P., Tollerud, E. J., et al. 2013, A&A, 558, A33
Baillard, A., Bertin, E., de Lapparent, V., et al. 2011, A&A, 532, A74
Bassa, C. G., Tendulkar, S. P., Adams, E. A. K., et al. 2017, ApJL, 843, L8
Bazin, G., Palanque-Delabrouille, N., Rich, J., et al. 2009, A&A, 499, 653
Beck, R., Szapudi, I., Flewelling, H., et al. 2021, MNRAS, 500, 1633
Becker, R. H., White, R. L., & Helfand, D. J. 1995, ApJ, 450, 559
Bell, M. E., Huynh, M. T., Hancock, P., et al. 2015, MNRAS, 450, 4221
Bernardi, M., Shankar, F., Hyde, J. B., et al. 2010, MNRAS, 404, 2087
Bhandari, S., Heintz, K. E., Aggarwal, K., et al. 2022, AJ, 163, 69
Bhandari, S., Sadler, E. M., Prochaska, J. X., et al. 2020, ApJL, 895, L37
Bhardwaj, M., Gaensler, B. M., Kaspi, V. M., et al. 2021a, ApJL, 910, L18
Bhardwaj, M., Kirichenko, A. Y., Michilli, D., et al. 2021b, ApJL, 919, L24
Bhardwaj, M., Lee, J., & Ji, K. 2024, arXiv:2408.01876
Bhardwaj, M., Palmese, A., Magaña Hernandez, I., D'Emilio, V., & Morisaki, S. 2023, arXiv:2306.00948
Bianchi, L., Shiao, B., & Thilker, D. 2017, ApJS, 230, 24
Blanchard, P. K., Berger, E., & Fong, W.-f. 2016, ApJ, 817, 144
Blanton, M. R., & Moustakas, J. 2009, ARA&A, 47, 159
Bloom, J. S., Kulkarni, S. R., & Djorgovski, S. G. 2002, AJ, 123, 1111
Bochenek, C. D., Ravi, V., Belov, K. V., et al. 2020, Natur, 587, 59
Bochenek, C. D., Ravi, V., & Dong, D. 2021, ApJL, 907, L31
Brennan, R., Pandya, V., Somerville, R. S., et al. 2015, MNRAS, 451, 2933
Brinchmann, J., Charlot, S., White, S. D. M., et al. 2004, MNRAS, 351, 1151
Buta, R. J. 2011, arXiv:1102.0550
Buta, R. J. 2019, MNRAS, 488, 590
Byler, N., Dalcanton, J. J., Conroy, C., & Johnson, B. D. 2017, ApJ, 840, 44
Caleb, M., Spitler, L. G., & Stappers, B. W. 2018, NatAs, 2, 839
Caleb, M., Stappers, B. W., Rajwade, K., & Flynn, C. 2019, MNRAS, 484, 5500
Calzetti, D., Armus, L., Bohlin, R. C., et al. 2000, ApJ, 533, 682
Cattorini, F., Gavazzi, G., Boselli, A., & Fossati, M. 2023, A&A, 671, A118
Chabrier, G. 2003, PASP, 115, 763
Chambers, K. C., Magnier, E. A., Metcalfe, N., et al. 2016, arXiv:1612.05560
Chang, Y.-Y., van der Wel, A., da Cunha, E., & Rix, H.-W. 2015, ApJS, 219, 8
Chatterjee, S., Law, C. J., Wharton, R. S., et al. 2017, Natur, 541, 58
Chawla, P., Kaspi, V. M., Ransom, S. M., et al. 2022, ApJ, 927, 35
CHIME/FRB Collaboration, Amiri, M., Andersen, B. C., et al. 2021, ApJS, 257, 59
CHIME/FRB Collaboration, Amiri, M., Bandura, K., et al. 2018, ApJ, 863, 48
CHIME/FRB Collaboration, Andersen, B. C., Bandura, K. M., et al. 2020, Natur, 587, 54
CHIME/FRB Collaboration, Andersen, B. C., Bandura, K., et al. 2019, ApJL, 885, L24
CHIME/FRB Collaboration, Andersen, B. C., Bandura, K., et al. 2023, ApJ, 947, 83
Chrimes, A. A., Levan, A. J., Groot, P. J., Lyman, J. D., & Nelemans, G. 2021, MNRAS, 508, 1929
Condon, J. J., Cotton, W., Greisen, E., et al. 1998, AJ, 115, 1693
Connor, L., Ravi, V., Catha, M., et al. 2023, ApJL, 949, L26
Conroy, C., Gunn, J. E., & White, M. 2009, ApJ, 699, 486
Cook, A. M., Bhardwaj, M., Gaensler, B. M., et al. 2023, ApJ, 946, 58
Cordes, J. M., & Lazio, T. J. W. 2002, arXiv:astro-ph/0207156
Cruces, M., Spitler, L. G., Scholz, P., et al. 2020, MNRAS, 500, 448
Cui, X.-H., Zhang, C.-M., Wang, S.-Q., et al. 2021, MNRAS, 500, 3275
Cutri, R. M., Wright, E. L., Conrow, T., et al. 2021, yCat, II/328
Dame, T. M., Hartmann, D., & Thaddeus, P. 2001, ApJ, 547, 792
Davari, R., Ho, L. C., & Peng, C. Y. 2016, ApJ, 824, 112
Delgado-Serrano, R., Hammer, F., Yang, Y. B., et al. 2010, A&A, 509, A78
Deng, X.-F. 2013, RAA, 13, 651
DESI Collaboration, Aghamousa, A., Aguilar, J., et al. 2016, arXiv:1611.00036
Domínguez Sánchez, H., Huertas-Company, M., Bernardi, M., Tuccillo, D., & Fischer, J. L. 2018, MNRAS, 476, 3661
Draine, B. T., & Li, A. 2007, ApJ, 657, 810
Driessen, L. N., Barr, E., Buckley, D., et al. 2024, MNRAS, 527, 3659
Driver, S. P., Andrews, S. K., Davies, L. J., et al. 2016, ApJ, 827, 108
Duarte Puertas, S., Vilchez, J. M., Iglesias-Páramo, J., et al. 2022, A&A, 666, A186
Dunnett, C. W., & Tamhane, A. C. 1992, JASA, 87, 162
Earl, N., Tollerud, E., O'Steen, R., et al. 2023, astropy/specutils: v1.10.0, Zenodo, doi:10.5281/zenodo.7803739
Eftekhari, T., & Berger, E. 2017, ApJ, 849, 162
Eldridge, J. J., Fraser, M., Smartt, S. J., Maund, J. R., & Crockett, R. M. 2013, MNRAS, 436, 774
Falcke, H., & Rezzolla, L. 2014, A&A, 562, A137
Fantin, N. J., Côté, P., McConnachie, A. W., et al. 2019, ApJ, 887, 148
Fender, R., Woudt, P. A., Corbel, S., et al. 2016, in MeerKAT Science: On the Pathway to the SKA, 13
Fong, W.-f., Dong, Y., Leja, J., et al. 2021, ApJL, 919, L23
Fong, W.-f., Nugent, A. E., Dong, Y., et al. 2022, ApJ, 940, 56
Fonseca, E., Andersen, B., Bhardwaj, M., et al. 2020, ApJ, 891, L6
Frane, A. V. 2015, Journal of Research Practice, 11, 2
Fryer, C., Benz, W., Herant, M., & Colgate, S. A. 1999, ApJ, 516, 892
Gaia Collaboration, Helmi, A., van Leeuwen, F., et al. 2018, yCat, J/A+A/616/A12
Galbany, L., Stanishev, V., Mourão, A. M., et al. 2014, A&A, 572, A38
Gallazzi, A., Charlot, S., Brinchmann, J., White, S. D. M., & Tremonti, C. A. 2005, MNRAS, 362, 41
Geda, R., Crawford, S. M., Hunt, L., et al. 2022, AJ, 163, 202
Glowacki, M., Lee-Waddell, K., Deller, A. T., et al. 2023, ApJ, 949, 25
Goldstein, A., Cleveland, W. H., & Kocevski, D. 2021, Fermi GBM Data Tools: v1.1.0, https://fermi.gsfc.nasa.gov/ssc/data/analysis/gbm
Gómez-González, V. M. A., Mayya, Y. D., & Rosa-González, D. 2016, MNRAS, 460, 1555
Gómez-Velarde, G., García-Alvarez, D., & Cabrerra-Lavers, A. 2016, in ASP Conf. Ser. 507, Multi-Object Spectroscopy in the Next Decade: Big Questions, Large Surveys, and Wide Fields, ed. I. Skillen, M. Balcells, & S. Trager (San Francisco, CA: ASP), 191
González-Serrano, J. I., Sánchez-Portal, M., Castañeda, H., et al. 2004, ExA, 18, 65
Gordon, A. C., Fong, W.-f., Kilpatrick, C. D., et al. 2023, ApJ, 954, 80
Graham, A. W., Driver, S. P., Petrosian, V., et al. 2005, AJ, 130, 1535
Graham, M. J., Kulkarni, S. R., Bellm, E. C., et al. 2019, PASP, 131, 078001
Grootes, M. W., Tuffs, R. J., Popescu, C. C., et al. 2017, AJ, 153, 111
Hale, C. L., McConnell, D., Thomson, A. J. M., et al. 2021, PASA, 38, e058
Harris, C. R., Millman, K. J., van der Walt, S. J., et al. 2020, Natur, 585, 357
Harris, W. E. 2010, arXiv:1012.3224
Hart, R. E., Bamford, S. P., Willett, K. W., et al. 2016, MNRAS, 461, 3663
Hashimoto, T., Goto, T., Chen, B. H., et al. 2022, MNRAS, 511, 1961
Hau, G. K. T., Ferguson, H. C., Lahav, O., & Lynden-Bell, D. 1995, MNRAS, 277, 125
Heintz, K. E., Prochaska, J. X., Simha, S., et al. 2020, ApJ, 903, 152
Hernández-Toledo, H. M., Vázquez-Mata, J. A., Martínez-Vázquez, L. A., Choi, Y.-Y., & Park, C. 2010, AJ, 139, 2525
Hillebrandt, W., & Niemeyer, J. C. 2000, ARA&A, 38, 191
Hinton, S. R., Davis, T. M., Lidman, C., Glazebrook, K., & Lewis, G. F. 2016, A&C, 15, 61
Hochberg, Y. 1988, Biometrika, 75, 800
Hong, T., Staveley-Smith, L., Masters, K. L., et al. 2019, MNRAS, 487, 2061

Huang, Y., & Hsu, J. C. 2007, Biometrika, 94, 965
Hudson, M. J., Harris, G. L., & Harris, W. E. 2014, ApJL, 787, L5
Hunter, J. D. 2007, CSE, 9, 90
Ibata, R. A., McConnachie, A., Cuillandre, J.-C., et al. 2017, ApJ, 848, 128
Ibik, A. L., Drout, M. R., Gaensler, B. M., et al. 2024, ApJ, 961, 99
Intema, H., Jagannathan, P., Mooley, K., & Frail, D. 2017, A&A, 598, A78
Jahns-Schindler, J. N., Spitler, L. G., Walker, C. R. H., & Baugh, C. M. 2023, MNRAS, 523, 5006
James, C. W. 2023, PASA, 40, e057
James, C. W., Prochaska, J. X., Macquart, J. P., et al. 2022, MNRAS, 509, 4775
Jarrett, T. H., Cluver, M. E., Brown, M. J. I., et al. 2020, yCat, J/ApJS/245/25
Jarrett, T. H., Cluver, M. E., Magoulas, C., et al. 2017, ApJ, 836, 182
Johnson, B. D., Leja, J. L., Conroy, C., & Speagle, J. S., 2019 Prospector: Stellar Population Inference from Spectra and SEDs, Astrophysics Source Code Library, ascl:1905.025
Josephy, A., Chawla, P., Curtin, A. P., et al. 2021, ApJ, 923, 2
Josephy, A., Chawla, P., Fonseca, E., et al. 2019, ApJL, 882, L18
Joye, W. A., & Mandel, E. 2003, in ASP Conf. Ser. 295, Astronomical Data Analysis Software and Systems XII, ed. H. E. Payne, R. I. Jedrzejewski, & R. N. Hook (San Francisco, CA: ASP), 489
Kaisina, E. I., Karachentsev, I. D., Makarov, D. I., & Kaisin, S. S. 2019, in IAU Symp. 344, Dwarf Galaxies: From the Deep Universe to the Present, ed. K. B. W. McQuinn & S. Stierwalt (Cambridge: Cambridge Univ. Press), 377
Karachentsev, I. D., & Kaisina, E. I. 2019, in IAU Symp. 344, Dwarf Galaxies: From the Deep Universe to the Present, ed. K. B. W. McQuinn & S. Stierwalt (Cambridge: Cambridge Univ. Press), 381
Kashiyama, K., Ioka, K., & Mészáros, P. 2013, ApJL, 776, L39
Kelly, P. L., & Kirshner, R. P. 2012, ApJ, 759, 107
Kelvin, L. S., Driver, S. P., Robotham, A. S. G., et al. 2014, MNRAS, 444, 1647
Kennicutt, R. C., Jr. 1998, ARA&A, 36, 189
Khrykin, I. S., Sorini, D., Lee, K.-G., & Davé, R. 2024, MNRAS, 529, 537
Kirsten, F., Marcote, B., Nimmo, K., et al. 2022, Natur, 602, 585
Kirsten, F., Ould-Boukattine, O., Herrmann, W., et al. 2024, NatAs, 8, 337
Kothes, R., Sun, X., Gaensler, B., & Reich, W. 2018, ApJ, 852, 54
Kourkchi, E., Tully, R. B., Eftekharzadeh, S., et al. 2020, ApJ, 902, 145
Kraft, R. P., Burrows, D. N., & Nousek, J. A. 1991, ApJ, 374, 344
Kremer, K., Fuller, J., Piro, A. L., & Ransom, S. M. 2023, MNRAS, 525, L22
Kremer, K., Piro, A. L., & Li, D. 2021a, ApJL, 917, L11
Kremer, K., Rui, N. Z., Weatherford, N. C., et al. 2021b, ApJ, 917, 28
Kriek, M., & Conroy, C. 2013, ApJL, 775, L16
Kuminski, E., & Shamir, L. 2016, ApJS, 223, 20
Lacy, M., Baum, S. A., Chandler, C. J., et al. 2016, AAS Meeting, 227, 324
Lanman, A. E., Andersen, B. C., Chawla, P., et al. 2022, ApJ, 927, 59
Lauberts, A. 1982, ESO/Uppsala Survey of the ESO(B) Atlas (Garching: ESO)
Law, C. J., Sharma, K., Ravi, V., et al. 2024, ApJ, 967, 29
Lawrence, A., Warren, S. J., Almaini, O., et al. 2007, MNRAS, 379, 1599
Lawrence, A., Warren, S. J., Almaini, O., et al. 2013, yCat, II/319
Law-Smith, J., Ramirez-Ruiz, E., Ellison, S. L., & Foley, R. J. 2017, ApJ, 850, 22
Lee-Waddell, K., James, C. W., Ryder, S. D., et al. 2023, PASA, 40, 29
Leja, J., Carnall, A. C., Johnson, B. D., Conroy, C., & Speagle, J. S. 2019a, ApJ, 876, 3
Leja, J., Johnson, B. D., Conroy, C., & van Dokkum, P. 2018, ApJ, 854, 62
Leja, J., Johnson, B. D., Conroy, C., van Dokkum, P. G., & Byler, N. 2017, ApJ, 837, 170
Leja, J., Johnson, B. D., Conroy, C., et al. 2019b, ApJ, 877, 140
Li, Y., & Zhang, B. 2020, ApJL, 899, L6
Liu, X. 2018, Ap&SS, 363, 242
Lorimer, D. R., Bailes, M., McLaughlin, M. A., Narkevic, D. J., & Crawford, F. 2007, Sci, 318, 777
Luo, R., Men, Y., Lee, K., et al. 2020, MNRAS, 494, 665
Macquart, J. P., Prochaska, J. X., McQuinn, M., et al. 2020, Natur, 581, 391
Mager, V. A., Conselice, C. J., Seibert, M., et al. 2018, ApJ, 864, 123
Mahony, E. K., Ekers, R. D., Macquart, J.-P., et al. 2018, ApJL, 867, L10
Mancini, C., Renzini, A., Daddi, E., et al. 2015, MNRAS, 450, 763
Mannings, A. G., Fong, W.-f., Simha, S., et al. 2021, ApJ, 917, 75
Marcote, B., Nimmo, K., Hessels, J. W. T., et al. 2020, Natur, 577, 190
Massey, P., Strobel, K., Barnes, J. V., & Anderson, E. 1988, ApJ, 328, 315
Massey, P., Strobel, K., Barnes, J. V., & Anderson, E. 1995, yCat, III/116
Mazzarella, J. M. & NED Team 2017, in IAU Symp. 325, Astroinformatics, ed. M. Brescia et al. (Cambridge: Cambridge Univ. Press), 379
McKinven, R. & CHIME/FRB Collaboration 2022, ATel, 15679, 1
Metzger, B. D., Berger, E., & Margalit, B. 2017, ApJ, 841, 14
Meyer, M. J., Zwaan, M. A., Webster, R. L., et al. 2004, MNRAS, 350 1195
Michilli, D., Bhardwaj, M., Brar, C., et al. 2023, ApJ, 950, 134
Michilli, D., Masui, K. W., Mckinven, R., et al. 2021, ApJ, 910, 147
Mitronova, S. N., Karachentsev, I. D., Karachentseva, V. E., Jarrett, T. H., & Kudrya, Y. N. 2004, BSAO, 57, 5
Mitronova, S. N., & Korotkova, G. G. 2015, AstBu, 70, 24
Moroianu, A., Wen, L., James, C. W., et al. 2023, NatAs, 7, 579
Most, E. R., Nathanail, A., & Rezzolla, L. 2018, ApJ, 864, 117
Murphy, E. J., Condon, J. J., Schinnerer, E., et al. 2011, ApJ, 737, 67
Muzzin, A., Marchesini, D., Stefanon, M., et al. 2013, ApJ, 777, 18
Nenkova, M., Sirocky, M. M., Ivezić, Ž., & Elitzur, M. 2008, ApJ, 685, 147
Nicholl, M., Williams, P. K. G., Berger, E., et al. 2017, ApJ, 843, 84
Nimmo, K., Hewitt, D. M., Hessels, J. W. T., et al. 2022, ApJL, 927, L3
Niu, C. H., Aggarwal, K., Li, D., et al. 2022, Natur, 606, 873
Ocker, S. K., Cordes, J. M., Chatterjee, S., & Gorsuch, M. R. 2022, ApJ, 934, 71
O'Connor, B., Troja, E., Dichiara, S., et al. 2022, MNRAS, 515, 4890
Oke, J. B. 1974, ApJS, 27, 21
Oke, J. B. 1990, AJ, 99, 1621
Olausen, S. A., & Kaspi, V. M. 2014, ApJS, 212, 6
Ould-Boukattine, O. S., Herrmann, W., Gawronski, M., et al. 2022, ATel, 15817, 1
Palaniswamy, D., Li, Y., & Zhang, B. 2018, ApJL, 854, L12
Pan, Y. C., Sullivan, M., Maguire, K., et al. 2014, MNRAS, 438, 1391
Pannella, M., Hopp, U., Saglia, R. P., et al. 2006, ApJL, 639, L1
Panther, F. H., Anderson, G. E., Bhandari, S., et al. 2023, MNRAS, 519, 2235
Pearlman, A. B., Scholz, P., Bethapudi, S., et al. 2023, arXiv:2308.10930
Peng, Y.-j., Lilly, S. J., Kovač, K., et al. 2010, ApJ, 721, 193
Perley, D. A., Fremling, C., Sollerman, J., et al. 2020, ApJ, 904, 35
Petroff, E., Hessels, J. W. T., & Lorimer, D. R. 2022, A&ARv, 30, 2
Pietka, M., Fender, R. P., & Keane, E. F. 2015, MNRAS, 446, 3687
Piro, A. L., & Kulkarni, S. R. 2013, ApJL, 762, L17
Planck Collaboration, Aghanim, N., Akrami, Y., et al. 2020, A&A, 641, A6
Platts, E., Weltman, A., Walters, A., et al. 2019, PhR, 821, 1
Pleunis, Z., Good, D. C., Kaspi, V. M., et al. 2021, ApJ, 923, 1
Price, D. C., Flynn, C., & Deller, A. 2021, PASA, 38, e038
Prochaska, J., Hennawi, J., Westfall, K., et al. 2020, JOSS, 5, 2308
Pruzhinskaya, M. V., Novinskaya, A. K., Pauna, N., & Rosnet, P. 2020, MNRAS, 499, 5121
Ravi, V. 2019, NatAs, 3, 928
Ravi, V., Catha, M., Chen, G., et al. 2023a, ApJL, 949, L3
Ravi, V., Catha, M., Chen, G., et al. 2023b, arXiv:2301.01000
Ravi, V., Law, C. J., Li, D., et al. 2022, MNRAS, 513, 982
Rengelink, R., Tang, Y., De Bruyn, A., et al. 1997, A&AS, 124, 259
Resmi, L., Vink, J., & Ishwara-Chandra, C. H. 2021, A&A, 655, A102
Robitaille, T., & Bressert, E., 2012 APLpy: Astronomical Plotting Library in Python, Astrophysics Source Code Library, ascl:1208.017
Ruiter, A. J., Belczynski, K., Sim, S. A., et al. 2010, in AIP Conf. Ser. 1314, Int. Conf. on Binaries: in Celebration of Ron Webbink's 65th Birthday, ed. V. Kalogera & M. van der Sluys (Melville, NY: AIP), 233
Sarin, N., Lasky, P. D., Vivanco, F. H., et al. 2022, PhRvD, 105, 083004
Saydjari, A. K., Schlafly, E. F., Lang, D., et al. 2023, ApJS, 264, 28
Schlafly, E. F., & Finkbeiner, D. P. 2011, ApJ, 737, 103
Scholz, P., Cook, A., Cruces, M., et al. 2020, ApJ, 901, 156
Schulze, S., Yaron, O., Sollerman, J., et al. 2021, ApJS, 255, 29
Scolnic, D. M., Jones, D. O., Rest, A., et al. 2018, ApJ, 859, 101
Scott, N., Brough, S., Croom, S. M., et al. 2017, MNRAS, 472, 2833
Seebeck, J., Ravi, V., Connor, L., et al. 2021, arXiv:2112.07639
Shannon, R. M., Macquart, J. P., Bannister, K. W., et al. 2018, Natur, 562, 386
Sharma, K., Somalwar, J., Law, C., et al. 2023, ApJ, 950, 175
Shimwell, T. W., Hardcastle, M. J., Tasse, C., et al. 2022, A&A, 659, A1
Shin, K., Masui, K. W., Bhardwaj, M., et al. 2023, ApJ, 944, 105
Simard, L., Mendel, J. T., Patton, D. R., Ellison, S. L., & McConnachie, A. W. 2011, ApJS, 196, 11
Sjolander, A., & Vansteelandt, S. 2019, Eur. J. Epidemiol., 34, 809
Skrutskie, M. F., Cutri, R. M., Stiening, R., et al. 2006, AJ, 131, 1163
Spanakis-Misirlis, A., 2021 FRBSTATS: A Web-based Platform for Visualization of Fast Radio Burst Properties, Astrophysics Source Code Library, ascl:2106.028
Speagle, J. S. 2020, MNRAS, 493, 3132
Svensson, K. M., Levan, A. J., Tanvir, N. R., Fruchter, A. S., & Strolger, L. G. 2010, MNRAS, 405, 57
Tendulkar, S. P., Bassa, C. G., Cordes, J. M., et al. 2017, ApJL, 834, L7

Tendulkar, S. P., Gil de Paz, A., Kirichenko, A. Y., et al. 2021, ApJL, 908, L12
The LIGO Scientific Collaboration, The Virgo Collaboration, The KAGRA Collaboration, et al. 2023, ApJ, 955, 155
Thornton, D., Stappers, B., Bailes, M., et al. 2013, Sci, 341, 53
Tody, D. 1986, Proc. SPIE, 627, 733
Tody, D. 1993, in ASP Conf. Ser. 52, Astronomical Data Analysis Software and Systems II, ed. R. J. Hanisch, R. J. V. Brissenden, & J. Barnes (San Francisco, CA: ASP), 173
Totani, T. 2013, PASJ, 65, L12
van den Bergh, S. 1979, JRASC, 73, 198
van den Bergh, S. 2009, ApJ, 702, 1502
Vasiliev, E. 2019, MNRAS, 484, 2832
Vidgen, B., & Yasseri, T. 2016, FrP, 4, 6
Vika, M., Vulcani, B., Bamford, S. P., Häußler, B., & Rojas, A. L. 2015, A&A, 577, A97
Vorontsov-Vel'Yaminov, B. A., & Arkhipova, V. P. 1962, MCG, C01, 0
Wenger, M., Ochsenbein, F., Egret, D., et al. 2000, A&AS, 143, 9
Whyte, L. F., Abraham, R. G., Merrifield, M. R., et al. 2002, MNRAS, 336, 1281
Wild, V., Taj Aldeen, L., Carnall, A., et al. 2020, MNRAS, 494, 529
Wright, E. L., Eisenhardt, P. R. M., Mainzer, A. K., et al. 2010, AJ, 140, 1868
Xu, H., Niu, J. R., Chen, P., et al. 2022, Natur, 609, 685
Xu, J., & Han, J. L. 2015, RAA, 15, 1629
Yamasaki, S., & Totani, T. 2020, ApJ, 888, 105
Yao, J., Manchester, R., & Wang, N. 2017, ApJ, 835, 29
Yaron, O., Ofek, E., Gal-Yam, A., & Sass, A. 2020, TNSAN, 70, 1
Yershov, V. N. 2014, Ap&SS, 354, 97
Zapartas, E., de Mink, S. E., Izzard, R. G., et al. 2017, A&A, 601, A29
Zhang, B. 2023, RvMP, 5, 035005
Zhang, G. Q., Yi, S. X., & Wang, F. Y. 2020, ApJ, 893, 44
Zhang, K., Li, L., Zhang, Z., et al. 2022, Univ, 8, 355
Zhao, Z. Y., Zhang, G. Q., Wang, Y. Y., Tu, Z.-L., & Wang, F. Y. 2021, ApJ, 907, 111
Zheng, Z., & Ramirez-Ruiz, E. 2007, ApJ, 665, 1220
Zhong, S.-Q., & Dai, Z.-G. 2020, ApJ, 893, 9